

Impurity and correlation effects on transport in one-dimensional quantum wires

T. Enss,¹ V. Meden,² S. Andergassen,¹ X. Barnabé-Thériault,^{2,*} W. Metzner,¹ and K. Schönhammer²

¹*Max-Planck-Institut für Festkörperforschung, Heisenbergstr. 1, D-70569 Stuttgart, Germany*

²*Institut für Theoretische Physik, Universität Göttingen, Friedrich-Hund-Platz 1, D-37077 Göttingen, Germany*

We study transport through a one-dimensional quantum wire of correlated fermions connected to semi-infinite leads. The wire contains either a single impurity or two barriers, the latter allowing for resonant tunneling. In the leads the fermions are assumed to be non-interacting. The wire is described by a microscopic lattice model. Using the functional renormalization group we calculate the linear conductance for wires of mesoscopic length and for all relevant temperature scales. For a single impurity, either strong or weak, we find power-law behavior as a function of temperature. In addition, we can describe the complete crossover from the weak- to the strong-impurity limit. For two barriers, depending on the parameters of the enclosed quantum dot, we find temperature regimes in which the conductance follows power-laws with “universal” exponents as well as non-universal behavior. Our approach leads to a comprehensive picture of resonant tunneling. We compare our results with those of alternative approaches.

I. INTRODUCTION

The interplay of static impurities and correlations in one-dimensional (1d) Fermi systems leads to a variety of surprising effects. A detailed understanding of the physics involved is interesting from the basic-science point of view as well as from the perspective of a possible application of 1d quantum wires in future nanoelectronics. In a 1d metallic system, correlations have a strong effect on the low-energy properties. Quite differently from the conventional Fermi-liquid behavior and even in the homogeneous case, physical properties at low energy scales follow power-laws, described by the Tomonaga-Luttinger liquid (TLL) phenomenology.¹ For spin-rotational invariant and spinless models the exponents can be expressed in terms of a single number, the interaction-dependent TLL parameter K .

A single static impurity in a TLL with repulsive interaction ($0 < K < 1$) leads to a dramatic modification of the low-energy physics as is obvious from lowest order perturbation theory in the strength of the impurity.²⁻⁵ More elaborate methods show that for vanishing energy scale s the conductance of such a system vanishes following a power-law.⁶⁻¹⁰ The scaling exponent $2\alpha_B$ is independent of the bare impurity strength and determined by the exponent $\alpha_B = 1/K - 1$ (for spinless fermions) of the one-particle spectral weight of a TLL close to an open boundary.⁶ For weak impurities the correction to the impurity free conductance scales as $s^{2(K-1)}$, which holds as long as the correction stays small. Assuming an infinite system the asymptotic low-energy properties have been investigated intensively within an integrable field theoretical model — the local sine-Gordon model (LSGM).^{6-8,10} For this model, with fixed K the conductance as a function of temperature follows one-parameter scaling for different strengths of the impurity. Similar results were obtained for a TLL connected by arbitrarily “smooth” (spatially adiabatic) contacts to semi-infinite Fermi-liquid leads.¹¹⁻¹⁶

Also transport through a double barrier enclosing a

quantum dot has been studied over the last few years using field theoretical models.^{6,17-27} Tuning the dot energies by a gate voltage V_g resonant tunneling can be achieved. For appropriately chosen dot parameters (dot size, barrier height) and as a function of temperature T the conductance G shows different temperature regimes with distinctive power-law scaling and exponents which can be expressed in terms of K .^{17,19-21,24-27} For the double-barrier problem no exactly solvable generic model is known and applying different approximate analytical^{17,19-21,24,25,27} and numerical²⁶ methods has not provided a consistent picture.

To study the effect of the interplay of correlations and impurities on transport on all relevant energy scales we use the functional renormalization group (fRG) method. The fRG can be applied directly to microscopic models. We consider the lattice model of spinless fermions with nearest-neighbor hopping t and nearest-neighbor interaction U . The impurities are modeled by either locally raising site energies or reducing hopping matrix elements across bonds. The fRG was recently introduced²⁸ as a new powerful tool for studying interacting Fermi systems. It provides a systematic way of resumming competing instabilities²⁹ and goes beyond simple perturbation theory even in problems which are not plagued by infrared divergences.³⁰ The fRG procedure we use starts from an exact hierarchy of differential flow equations for the one-particle irreducible vertex functions,³¹⁻³³ as e.g. the self-energy and the effective two-particle interaction. It is derived by replacing the free propagator by a propagator depending on an infrared cutoff Λ and taking the derivative of the generating functional with respect to Λ .

At $T = 0$ we introduced earlier two truncation schemes which led to a manageable number of coupled equations.³⁴⁻³⁶ The flow of the self-energy, which in particular encodes the renormalized impurity potential, is fully taken into account, while the two-particle vertex is parametrized by a single flowing coupling constant.³⁶ The bare two-particle interaction U is taken as a small parameter, but the impurities can have arbitrary strength and

shape. We are thus in a position to study the single- and double-barrier problem by applying the same approximate method. For weak and strong single impurities the flow equations can be solved analytically.³⁵ The results are consistent with the above mentioned power-law scaling of the conductance. For general parameters, in particular in the double barrier case, we solved the coupled differential equations numerically which at $T = 0$ can easily be done for systems of up to $N = 10^7$ lattice sites. Using the fRG we previously studied the one-particle spectral function close to a single impurity,³⁴⁻³⁶ the decay of density (Friedel-) oscillations off an impurity,³⁶ and the persistent current in mesoscopic rings pierced by a magnetic flux.³⁷ For these observables we recovered the expected “universal” power-laws with exponents which for $1/2 \leq K < 1$ ($K \rightarrow 1$ for $U \rightarrow 0$) turned out to be in good agreement with the ones known from the LSGM. In addition it was shown that the asymptotic behavior typically sets in on very small energy scales and for very large systems, except for very strong bare impurities. Within our approximation, in the calculation of various observables we have to solve as a last step the problem of a non-interacting fermion moving in the renormalized impurity potential. This mapping on an effective one-particle problem is helpful for the understanding of the observed effects.

In a short publication we previously discussed the transport for the single-barrier case.³⁸ The results were obtained after supplementing the N -site wire of interacting fermions (called the “interacting wire” in the following) by 1d semi-infinite leads. We studied the $T = 0$ behavior as a function of $1/N$. For “smooth” contacts between the leads and the interacting wire our data for different impurity strengths and inverse system sizes collapse onto a single curve after applying a one-parameter scaling ansatz. This shows that even a small bare impurity leads to a vanishing conductance in the limit $N \rightarrow \infty$. At $K = 1/2$ the one-parameter scaling function of the infinite LSGM is known analytically.^{6,10} Up to a small error our rescaled data fall onto this curve. As an additional benchmark for small N we compared the fRG approximation for the conductance with results of density-matrix renormalization group (DMRG) calculations.^{38,39} These tests lead us to conclude that our approximate method works reliably for interactions in the range $1/2 \leq K \leq 1$. In addition, the collapse of our fRG data onto the $K = 1/2$ local sine-Gordon scaling function provides an indication that the low-energy physics of the LSGM can indeed be found in a large class of models of inhomogeneous, one-dimensional, and correlated electron systems, which is not obvious *a priori*.

In the present publication we extend the fRG scheme of Ref. 36 to finite temperatures. As in any experimental system the bandwidth B and the inverse of the wire length set upper and lower bounds for the possible “universal” scaling behavior of the conductance. This has to be contrasted to studies of field-theoretical models with $B = \infty$ and (in most cases) $1/N = 0$. We calculate G

on all temperature scales. Depending on the bare impurity and interaction strength an asymptotic low-energy regime might not be reachable in experiments on finite wires. For finite T we consider up to $N = 10^4$ sites. For typical lattice constants this leads to interacting wires in the micrometer range, roughly corresponding to quantum wires accessible to transport experiments. Within the last few years, transport properties were measured in different, effectively 1d mesoscopic wires.⁴¹⁻⁴⁸

Although in many respects our model is more realistic than the field-theoretical models studied so far, important ingredients for an appropriate description of the experimental situation are missing, as e.g. the spin degree of freedom, higher-dimensional leads, and realistic contacts. In the present paper we therefore refrain from a detailed comparison of our results to experiments. Later, we briefly comment on certain aspects of the experimental results and discuss the possibility of extending our method to treat models closer to experimental systems.

In the two limits of weak and strong impurities we recover the expected power-law scaling of $G(T)$ with exponents which are in good agreement with the ones known from the LSGM. We show that one-parameter scaling is achieved. We also present results for attractive interactions with $U < 0$ and $K > 1$. Based on our findings we discuss the accuracy of our approximation scheme in detail. We investigate the relation between our approach and a “leading-log” resummation for the effective transmission at the chemical potential introduced in Ref. 9. We then consider the double-barrier problem. Within a single approximation scheme all relevant temperature regimes can be investigated, leading to a comprehensive picture. We compare our findings to results that have been obtained for restricted temperature regimes by applying alternative approximate techniques and a numerical method to field-theoretical models. A brief account of results for resonant tunneling in the double-barrier problem obtained from the fRG has been presented earlier, focusing on the scaling of the peak conductance for symmetric barriers.⁴⁰

This paper is organized as follows. In Sect. II we introduce the model considered. In Sect. III results of single-particle scattering theory are derived. They are useful for the understanding of our findings for the conductance. The details of the fRG method are presented in Sect. IV. We discuss the general approximation scheme and describe how the fRG is extended to finite T and to the study of transport. In Sect. V we present our results for the transport in the presence of a single impurity as well as through a double barrier. We conclude with a summary and an outlook in Sect. VI. In the appendix we briefly describe the relation between the imaginary part of the self-energy and the occurrence of current-vertex corrections in a Landauer-Büttiker-type expression for the conductance.

II. THE MODEL

We consider spinless fermions on a lattice with nearest-neighbor interaction supplemented by various types of impurities. The Hamiltonian reads

$$H = H_{\text{kin}} + H_{\text{int}} + H_{\text{imp}}. \quad (1)$$

The kinetic energy is given by nearest-neighbor hopping with an amplitude t ,

$$H_{\text{kin}} = -t \sum_{j=-\infty}^{\infty} (c_{j+1}^\dagger c_j + c_j^\dagger c_{j+1}), \quad (2)$$

where we used standard second-quantized notation with c_j^\dagger and c_j being creation and annihilation operators on site j , respectively.

The part of the Hamiltonian containing the interaction reads

$$H_{\text{int}} = \sum_{j=1}^{N-1} U_{j,j+1} [n_j - \nu(n, U)] [n_{j+1} - \nu(n, U)], \quad (3)$$

with the local density operator $n_j = c_j^\dagger c_j$. The interaction acts only between the bonds of the sites 1 to N , which define the interacting wire. The interaction $U_{j,j+1}$ between electrons on sites j and $j+1$ is allowed to depend on the position. As discussed in Refs. 38 and 39 in the absence of a one-particle impurity potential, turning on the interaction sharply leads to a reduction of the conductance compared to e^2/h .⁴⁹ As in the other theoretical studies mentioned we here avoid this effect by modeling ‘‘perfect’’ contacts. To achieve this $U_{j,j+1}$ is taken as a smoothly increasing function of j starting from zero at the bond (1, 2) and approaching a constant bulk value U over a sufficiently large number of bonds. Equally, the $U_{j,j+1}$ are switched off close to the bond $(N-1, N)$. The results are independent of the detailed shape of the envelope function as long as it is sufficiently smooth. The larger N the ‘‘smoother’’ $U_{j,j+1}$ has to be chosen. More explicitly we here take (N even, $j = 1, \dots, N/2$)

$$U_{j,j+1} = U \frac{\arctan[s(j - j_s)] - \arctan[s(1 - j_s)]}{\arctan[s(N/2 - j_s)] - \arctan[s(1 - j_s)]} \quad (4)$$

for the left part of the interacting wire and likewise for the right. For odd N a similar function is used. The parameters s and j_s are chosen such that in the absence of any impurity for $T = 0$ we find $1 - G/(e^2/h) < 10^{-6}$. To achieve this for the N considered here $j_s = 56$ and $s \approx 1/4$ is sufficient. The two regions of the lattice with $j < 1$ and $j > N$ constitute the two semi-infinite leads.

In Eq. (3) we shifted n_j by a parameter $\nu(n, U)$, which depends on the filling factor n and U . This is equivalent to introducing an additional one-particle potential in the interacting part of the system. The parameter $\nu(n, U)$ is chosen in such a way that the density in the interacting wire acquires the desired value n .

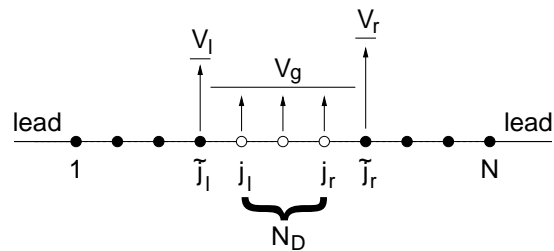


FIG. 1: Schematic plot of the quantum dot situation, where the barriers are modeled by two site impurities.

The general form of the impurity part of the Hamiltonian is written as

$$H_{\text{imp}} = \sum_{j,j'} V_{j,j'} c_j^\dagger c_{j'}, \quad (5)$$

where $V_{j,j'}$ is a static potential. Site impurities are given by a local potential

$$V_{j,j'} = V_j \delta_{j,j'}. \quad (6)$$

In our study of the effect of a single barrier we mainly consider a site impurity located far away from both leads on site j_0 with $j_0 \gg 1$ and $N - j_0 \gg 1$,

$$V_j = V \delta_{j,j_0}. \quad (7)$$

In the discussion of resonant tunneling two site impurities of strengths V_l and V_r on the sites $\tilde{j}_l = j_l - 1$ and $\tilde{j}_r = j_r + 1$ constitute the barriers, with $j_l \gg 1$ and $N - j_r \gg 1$. The N_D sites between j_l and j_r define the quantum dot with $j_r - j_l + 1 = N_D \geq 1$. The effect of a gate voltage is described by a constant V_g on sites j_l to j_r . This situation is depicted in Fig. 1. We also consider hopping impurities described by non-local potentials

$$V_{j,j'} = V_{j',j} = -t_{j,j+1} \delta_{j',j+1} \quad (8)$$

as barriers. For the special case of a single hopping impurity,

$$t_{j,j+1} = (t' - t) \delta_{j,j_0}, \quad (9)$$

the hopping amplitude t is replaced by t' on the bond linking the sites j_0 and $j_0 + 1$. In the double-barrier problem we consider a hopping t_l across the bond (\tilde{j}_l, j_l) and t_r across (j_r, \tilde{j}_r) . For small t_l and t_r also the interactions across the bonds (\tilde{j}_l, j_l) and (j_r, \tilde{j}_r) , i.e. $U_{\tilde{j}_l, j_l}$ and U_{j_r, \tilde{j}_r} , are assumed to be reduced. In the following we set the bulk hopping amplitude t equal to one, i.e. all energies are given in units of t . This leads to the non-interacting dispersion $\varepsilon_k = -2 \cos k$ and bandwidth $B = 4$. The lattice constant is set to 1.

The homogeneous model $H = H_{\text{kin}} + H_{\text{int}}$ with a constant interaction U across all bonds (not only the ones within $[1, N]$) can be solved exactly by Bethe ansatz.⁵⁰ It shows TLL behavior for all particle densities n and

any interaction strength except at half filling for $|U| > 2$. The U - and n -dependent TLL parameter K can be determined solving coupled integral equations,⁵⁰ which in the half-filled case can be done analytically with the result

$$K = \left[\frac{2}{\pi} \arccos \left(-\frac{U}{2} \right) \right]^{-1}, \quad (10)$$

for $|U| \leq 2$.

We compute the conductance of the above models in the linear-response regime. For $T = 0$ the fRG flow equations can be solved numerically for interacting wires as large as $N = 10^7$ lattice sites. For finite T we treat systems with up to $N = 10^4$ sites.

III. SCATTERING ON ONE-DIMENSIONAL LATTICES

The truncation of our fRG flow equations leads to a scattering problem of non-interacting fermions in an effective potential given by the non-trivial spatial dependence of the self-energy on sites 1 to N .^{34–36} It is thus useful to present some results for the scattering in a 1d system with an arbitrary (non-local) potential in a finite segment of the infinite wire. The results are important for the understanding of how the fRG based approximation scheme is set up and how the conductance is calculated within this scheme (see Sect. IV). In the first subsection we focus on this aspect. In the second more technical subsection we derive relations which can be used to gain a deeper understanding of our results for the conductance presented in Sect. V. In order to make this section self-contained we include short derivations of well-known results, as e.g. Eq. (15).

A. General relations

The single-particle Hamiltonian $H_{1p} = H_0 + V_{LR}$ we consider in this section reads

$$\begin{aligned} H_0 &= - \sum_{j=-\infty}^0 (|j-1\rangle\langle j| + \text{h.c.}) \\ &\quad - \sum_{j=N+1}^{\infty} (|j\rangle\langle j+1| + \text{h.c.}) + H_s \\ V_{LR} &= -t_L (|0\rangle\langle 1| + \text{h.c.}) - t_R (|N\rangle\langle N+1| + \text{h.c.}), \end{aligned} \quad (11)$$

where $|j\rangle$ denotes the state in which the fermion is centered at lattice site j . Here H_s is a general single-particle Hamiltonian in the scattering segment from site 1 to N which is connected to ideal leads with nearest-neighbor hopping $t = 1$. The hopping matrix elements t_L and t_R connecting the three parts described by H_0 are assumed to be real.

There are two ways to describe the scattering problem. In the usual approach the ideal infinite system is used as the unperturbed system and the deviations are treated as the perturbation. In Eq. (11) the grouping has been made differently. The disconnected system “left lead – scattering region – right lead” is described by H_0 and the connections proportional to t_L and t_R present the perturbation in the construction of the scattering states $|k, a\pm\rangle$ ⁵¹

$$\begin{aligned} |k, a\pm\rangle &= \lim_{\eta \rightarrow 0} \frac{\pm i\eta}{\varepsilon_k - H_{1p} \pm i\eta} |k, a\rangle \\ &= \lim_{\eta \rightarrow 0} \pm i\eta G(\varepsilon_k \pm i\eta) |k, a\rangle \\ &= |k, a\rangle + G(\varepsilon_k \pm i0) V_{LR} |k, a\rangle. \end{aligned} \quad (12)$$

Here the index a stands for L, R and the unperturbed states $|k, L(R)\rangle$ are standing waves in the left (right) semi-infinite lead, e.g. for $j \leq 0$

$$\begin{aligned} \langle j|k, L\rangle &= \sqrt{\frac{2}{\pi}} \sin [k(j-1)] \\ &= \frac{-i}{\sqrt{2\pi}} \left[e^{ik(j-1)} - e^{-ik(j-1)} \right]. \end{aligned} \quad (13)$$

In this section $G(z)$ denotes the resolvent matrix with respect to H_{1p} . With the above normalization of the standing waves, $\langle k, a|k', a'\rangle = \delta_{a,a'} \delta(k - k')$ holds. For $j > N$ the scattering state $|k, L+\rangle$ has components

$$\begin{aligned} \langle j|k, L+\rangle &= -\langle j|G(\varepsilon_k + i0)|1\rangle t_L \langle 0|k, L\rangle \\ &= \langle j|G_0(\varepsilon_k + i0)|N+1\rangle t_R \\ &\quad \times \langle N|G(\varepsilon_k + i0)|1\rangle t_L \langle 0|k, L\rangle. \end{aligned} \quad (14)$$

In the second equation we used $G = G_0 + G_0 V_{LR} G$ with $G_0(z) = (z - H_0)^{-1}$. The resolvent matrix element of the semi-infinite chain in Eq. (14) is given by⁵²

$$\langle j|G_0(\varepsilon_k + i0)|N+1\rangle = -e^{ik(j-N)},$$

which shows that $\langle j|k, L+\rangle$ is in fact an outgoing plane wave. From Eqs. (13) and (14) the transmission amplitude $t(\varepsilon_k)$ can be read off. The corresponding probability is given by

$$|t(\varepsilon_k)|^2 = 4t_L^2 t_R^2 \sin^2 k |\langle N|G(\varepsilon_k + i0)|1\rangle|^2. \quad (15)$$

This is a very important relation, as in the Landauer-Büttiker formula⁵³ the transmission probability directly determines the linear conductance $G(T)$ of non-interacting fermions at temperature T . For spinless fermions on the lattice it reads

$$G(T) = \frac{e^2}{h} \int_{-B/2}^{B/2} \left(-\frac{df}{d\varepsilon} \right) |t(\varepsilon)|^2 d\varepsilon, \quad (16)$$

where $f(\varepsilon) = 1/(e^{\beta(\varepsilon-\mu)} + 1)$ is the Fermi function with $\beta = 1/T$ and μ the chemical potential. The Boltzmann constant k_B is set to 1. If the fRG flow is integrated for

a finite temperature and a finite interacting wire the self-energy is T - and N -dependent, i.e. H_s and therefore also the transmission probability $|t(\varepsilon)|^2$ depends on temperature and wire length. In the notation used in this section these additional dependences are left implicit.

For the further discussion of the resolvent matrix element in Eq. (15) the relation⁵¹

$$PG(z)P = \left[zP - PH_{1p}P - PH_{1p}Q(zQ - QH_{1p}Q)^{-1}QH_{1p}P \right]^{-1}, \quad (17)$$

where P and Q are projectors with $P + Q = \mathbf{1}$, is used several times. With this projection formula the calculation of $\langle N|G(\varepsilon_k + i0)|1\rangle$ for the infinite system can be reduced to the problem of inverting an $N \times N$ -matrix. With the definition $P_s = \sum_{j=1}^N |j\rangle\langle j|$ one obtains

$$\langle N|G(z)|1\rangle = \langle N| [zP_s - H_s^{\text{eff}}(z)]^{-1} |1\rangle, \quad (18)$$

where G_b^0 is the diagonal element of the resolvent of the semi-infinite chain at the boundary and

$$H_s^{\text{eff}}(z) = H_s + G_b^0(z) (t_L^2 |1\rangle\langle 1| + t_R^2 |N\rangle\langle N|).$$

For energies inside the band G_b^0 is given by

$$G_b^0(\varepsilon + i0) = -e^{ik(\varepsilon)} = (\varepsilon - i\sqrt{4 - \varepsilon^2})/2.$$

In our fRG description of interacting fermions the ‘‘scattering segment’’ $[1, N]$ is defined by the part of the wire where interactions are present.

B. The double barrier problem

As one of the problems in our paper we discuss transport through a quantum dot with N_D sites extending from $j_l \gg 1$ to j_r with $N - j_r \gg 1$, where $j_r = j_l + N_D - 1$. For the sites neighboring the dot we use the indices \tilde{j}_a ($a = l, r$). In H_s the (real) hopping matrix elements from site \tilde{j}_l to j_l are denoted by \tilde{t}_l and from j_r to \tilde{j}_r by \tilde{t}_r .⁵⁴ Proceeding similarly as in Eq. (14) one can express $G_{N,1} = \langle N|G|1\rangle$ as

$$G_{N,1} = -G_{N,\tilde{j}_l} \tilde{t}_l G_{\tilde{j}_l,1}^{0,l} = G_{N,\tilde{j}_r}^{0,r} \tilde{t}_r G_{j_r,\tilde{j}_r} \tilde{t}_l G_{\tilde{j}_l,1}^{0,l}, \quad (19)$$

where

$$G^{0,a}(z) = [z - H_{1,p}(\tilde{t}_a = 0)]^{-1}$$

is the resolvent for the system cut into two pieces by putting $\tilde{t}_a = 0$. Since $G^{0,a}$ enters the expressions for the transmission probability derived below, we emphasize that $G^{0,a}$ is not the Green function for the Hamiltonian (11) but an auxiliary Green function. Using the projection technique again the problem of calculating G_{j_r,j_l} can be reduced to the inversion of an $N_D \times N_D$ matrix. With $P_{\text{dot}} = \sum_{j=j_l}^{j_r} |j\rangle\langle j|$ one obtains

$$P_{\text{dot}}G(z)P_{\text{dot}} = [zP_{\text{dot}} - P_{\text{dot}}H_sP_{\text{dot}} - H_b(z)]^{-1}, \quad (20)$$

where the boundary term is given by

$$H_b(z) = \Gamma_l(z)|j_l\rangle\langle j_l| + \Gamma_r(z)|j_r\rangle\langle j_r|, \quad (21)$$

with

$$\Gamma_a(z) = \tilde{t}_a^2 G_{\tilde{j}_a, \tilde{j}_a}^{0,a}(z).$$

As the information from outside the dot is contained in Γ_a it is desirable to express the conductance also in terms of these functions. If one defines the projector $P_l = \sum_{j=1}^{\tilde{j}_l} |j\rangle\langle j|$ and using Eq. (18) one can derive the following identity for $G_{P_l P_l}^{0,l} = P_l G^{0,l} P_l$,

$$G_{P_l P_l}^{0,l}(\varepsilon + i0) - G_{P_l P_l}^{0,l}(\varepsilon - i0) = -it_L^2 \sqrt{4 - \varepsilon^2} G_{P_l P_l}^{0,l}(\varepsilon + i0) |1\rangle\langle 1| G_{P_l P_l}^{0,l}(\varepsilon - i0). \quad (22)$$

The \tilde{j}_l, \tilde{j}_l matrix element of this equation relates $|G_{\tilde{j}_l,1}^{0,l}|^2$ to the imaginary part of $G_{\tilde{j}_l, \tilde{j}_l}^{0,l}$. With the analogous relation for the right neighbor of the dot one finally obtains using Eqs. (15) and (19)

$$|t(\varepsilon)|^2 = 4\Delta_l(\varepsilon)\Delta_r(\varepsilon)|G_{j_r, \tilde{j}_l}(\varepsilon + i0)|^2. \quad (23)$$

Here we have decomposed

$$\Gamma_a(\varepsilon + i0) = \Omega_a(\varepsilon) - i\Delta_a(\varepsilon),$$

with Ω_a and Δ_a real functions. This equation is a useful generalization of Eq. (15).

The explicit result for the transmission probability is simplest for the case $N_D = 1$. Then $H_{\text{dot}} = P_{\text{dot}}H_sP_{\text{dot}}$ consists of a single term⁵⁵ $\tilde{V}_g|j_l\rangle\langle j_l|$ and one obtains the generalized Breit-Wigner form⁵¹

$$|t(\varepsilon)|^2 = \frac{4\Delta_l(\varepsilon)\Delta_r(\varepsilon)}{\left[\varepsilon - \tilde{V}_g - \Omega_l(\varepsilon) - \Omega_r(\varepsilon) \right]^2 + [\Delta_l(\varepsilon) + \Delta_r(\varepsilon)]^2}. \quad (24)$$

In all cases discussed in this paper a resonance occurs at the energy ε_R , where $\varepsilon_R - \tilde{V}_g - \Omega_l(\varepsilon_R) - \Omega_r(\varepsilon_R)$ vanishes. Only for a symmetric dot with $\Delta_l = \Delta_r = \Delta$ the peak value is given by one, i.e. perfect transmission. Later Eq. (24) will also be used for the understanding of the conductance in the presence of a single site impurity.

For general dot size, G_{j_r, j_l} can be expressed in terms of the Γ_a and the resolvent of the isolated dot,

$$\bar{G}^0(z) = (zP_{\text{dot}} - H_{\text{dot}})^{-1},$$

using the special form of H_b in Eq. (21)

$$G_{j_r, j_l} = \frac{\bar{G}_{j_r, j_l}^0}{(1 - \Gamma_l \bar{G}_{j_l, j_l}^0)(1 - \Gamma_r \bar{G}_{j_r, j_r}^0) - \Gamma_l \Gamma_r \bar{G}_{j_l, j_r}^0 \bar{G}_{j_r, j_l}^0}. \quad (25)$$

For $|\Gamma_l|, |\Gamma_r| \ll 1$ one can have N_D narrow resonances which have the generalized Breit-Wigner form as in

Eq. (24). This follows from Eq. (25) by using the spectral representation

$$\bar{G}_{j,j'}^0(z) = \sum_{\alpha=1}^{N_D} \frac{\langle j|\varepsilon_\alpha\rangle\langle\varepsilon_\alpha|j'\rangle}{z - \varepsilon_\alpha}, \quad (26)$$

where the $|\varepsilon_\alpha\rangle$ are the eigenstates of H_{dot} . The corresponding eigenvalues ε_α depend linearly on \tilde{V}_g . For dots weakly coupled to the rest of the system the poles in Eq. (26) lead to narrow resonances in G_{j_r,j_l} . For energies close to ε_α the resolvent matrix elements $\bar{G}_{j,j'}^0$ can be replaced by the corresponding single-pole term. Then the terms quadratic in \bar{G}^0 in the denominator of Eq. (25) cancel and for $\varepsilon \approx \varepsilon_\alpha$ one obtains

$$|t(\varepsilon)|^2 \approx \frac{4\Delta_l^{(\alpha)}(\varepsilon)\Delta_r^{(\alpha)}(\varepsilon)}{\left[\varepsilon - \varepsilon_\alpha - \Omega_l^{(\alpha)}(\varepsilon) - \Omega_r^{(\alpha)}(\varepsilon)\right]^2 + \left[\Delta_l^{(\alpha)}(\varepsilon) + \Delta_r^{(\alpha)}(\varepsilon)\right]^2}, \quad (27)$$

where $\Delta_a^{(\alpha)}(\varepsilon) = |\langle j_a|\varepsilon_\alpha\rangle|^2\Delta_a(\varepsilon)$ and correspondingly for $\Omega_a^{(\alpha)}$. The factor $|\langle j_a|\varepsilon_\alpha\rangle|^2$ is typically of order $1/N_D$ and the widths of the resonances are reduced by this factor compared to the $N_D = 1$ dot. As the separation of the resonances is of order B/N_D the generalized Breit-Wigner form as in Eq. (24) holds for $|\Gamma_l|, |\Gamma_r| \ll 1$. This can be fulfilled for $\tilde{t}_l^2, \tilde{t}_r^2 \ll 1$ or for large site impurities at sites \tilde{j}_l and \tilde{j}_r (see below). If $\Gamma_a(\varepsilon)$ is assumed to be slowly varying over energies of the resonance width the integrated weight w_α of the Lorentzian resonance near ε_α is given by

$$w_\alpha \approx 4\pi[1/\Delta_l^{(\alpha)}(\varepsilon_\alpha) + 1/\Delta_r^{(\alpha)}(\varepsilon_\alpha)]^{-1}.$$

Here we have assumed that $1 - (\Omega_a^{(\alpha)})' \approx 1$, which holds for large dots with separated resonances.

Using the general projection formula (17) a relation between the diagonal matrix elements of the auxiliary Green function $G_{\tilde{j}_a,\tilde{j}_a}^{0,a}$ to the left and right of the dot [entering Eqs. (24) and (27)] and the corresponding matrix elements of the exact Green function $G_{\tilde{j}_a,\tilde{j}_a}$ can be derived. For general dot size and with $\bar{a} \neq a$ one obtains

$$G_{\tilde{j}_a,\tilde{j}_a} = \frac{(1 - \Gamma_{\bar{a}}\bar{G}_{\tilde{j}_a,\tilde{j}_a}^0)G_{\tilde{j}_a,\tilde{j}_a}^{0,a}}{(1 - \Gamma_l\bar{G}_{\tilde{j}_l,\tilde{j}_l}^0)(1 - \Gamma_r\bar{G}_{\tilde{j}_r,\tilde{j}_r}^0) - \Gamma_l\Gamma_r\bar{G}_{\tilde{j}_l,\tilde{j}_r}^0\bar{G}_{\tilde{j}_r,\tilde{j}_l}^0} \approx \frac{\left[\varepsilon - \varepsilon_\alpha - \Omega_{\bar{a}}^{(\alpha)}(\varepsilon) + i\Delta_{\bar{a}}^{(\alpha)}(\varepsilon)\right]G_{\tilde{j}_a,\tilde{j}_a}^{0,a}(\varepsilon + i0)}{\varepsilon - \varepsilon_\alpha - \Omega_l^{(\alpha)}(\varepsilon) - \Omega_r^{(\alpha)}(\varepsilon) + i\left[\Delta_l^{(\alpha)}(\varepsilon) + \Delta_r^{(\alpha)}(\varepsilon)\right]}, \quad (28)$$

where the second line holds for $z = \varepsilon + i0 \approx \varepsilon_\alpha$ in the case of dots which are only weakly coupled to the rest of the system.

For the interpretation of the temperature dependence of the conductance of a dot with narrow resonances in the regime $B/N_D \ll T \ll B$ also the first equality in

Eq. (19) is useful. Applying the general projection formula (17) yields

$$G_{N,j_l} = \frac{G_{N,j_l}^{0,l}}{1 - \tilde{t}_l^2 G_{\tilde{j}_l,\tilde{j}_l}^{0,l} G_{j_l,j_l}^{0,l}}.$$

With Eq. (22) and the corresponding relation for $G_{N,j_l}^{0,l}$ one obtains another exact relation for the transmission probability

$$|t(\varepsilon)|^2 = \frac{4\Delta_l(\varepsilon)\text{Im}G_{\tilde{j}_l,\tilde{j}_l}^{0,l}(\varepsilon + i0)}{\left|1 - \Gamma_l(\varepsilon + i0)G_{\tilde{j}_l,\tilde{j}_l}^{0,l}(\varepsilon + i0)\right|^2}. \quad (29)$$

If $|\Gamma_l| \ll 1$ but $|\Gamma_r| \approx 1$ no resonances occur and perturbation theory in Γ_l is possible. Putting the denominator in Eq. (29) equal to 1 leads to the ‘‘golden-rule’’ approximation. The conductance for this ‘‘single-impurity case’’ is then to leading order in \tilde{t}_l^2 given by

$$g_l(T) = G_l(T)\frac{h}{e^2} \approx 4\tilde{t}_l^2 \int_{-B/2}^{B/2} \left(-\frac{df}{d\varepsilon}\right) \text{Im}G_{\tilde{j}_l,\tilde{j}_l}^{0,l}(\varepsilon + i0) \times \text{Im}G_{j_l,j_l}^{0,l}(\varepsilon + i0)d\varepsilon. \quad (30)$$

We now return to the dot situation with narrow resonances. Its simplest realization is given by two hopping impurities with $\tilde{t}_l^2, \tilde{t}_r^2 \ll 1$ in an otherwise perfect lattice. Then the $G_{\tilde{j}_a,\tilde{j}_a}^{0,a}$ and $|\langle j_a|\varepsilon_\alpha\rangle|^2$ for $a = l, r$ are identical and the expression for the weights of the resonances simplifies to

$$w_\alpha \approx 4\pi \frac{|\langle j_l|\varepsilon_\alpha\rangle|^2 |\text{Im}G_{\tilde{j}_l,\tilde{j}_l}^{0,l}(\varepsilon_\alpha)|}{\tilde{t}_l^{-2} + \tilde{t}_r^{-2}}.$$

For $B/N_D \ll T \ll B$ the transmission probability $|t(\varepsilon)|^2$ in the Landauer-Büttiker formula (16) can approximately be replaced by $\sum_\alpha w_\alpha \delta(\varepsilon - \varepsilon_\alpha)$. This yields

$$g_{\text{dot}}(T) \approx 4 \left[\frac{1}{\tilde{t}_l^2} + \frac{1}{\tilde{t}_r^2}\right]^{-1} \int_{-B/2}^{B/2} \left(-\frac{df}{d\varepsilon}\right) \text{Im}G_{\tilde{j}_l,\tilde{j}_l}^{0,l}(\varepsilon + i0) \times \text{Im}\bar{G}_{j_l,j_l}^0(\varepsilon + i0)d\varepsilon. \quad (31)$$

The integrands in Eqs. (30) and (31) differ in the last factor. For the simple example with $\tilde{t}_l^2 \ll 1$ in an otherwise perfect lattice $G_{j_l,j_l}^{0,l}$ is just the boundary Green function G_b^0 of a semi-infinite lattice. For $N_D \gg 1$ and $\tilde{t}_r^2 \ll 1$ the imaginary part of the boundary Green function $\text{Im}\bar{G}_{j_l,j_l}^0$ of the dot can for the purpose of integration in Eq. (31) be approximately replaced by $\text{Im}G_b^0$. In Sect. V we encounter more interesting realizations for which the simplified expression for w_α as well as this replacement can be used. Comparison of Eqs. (30) and (31) then shows that in the ‘‘high-temperature regime’’ $B/N_D \ll T \ll B$ the conductance of the dot can be obtained by adding

resistances for the single-impurity problems (Kirchhoff's law) described by Eq. (30),

$$\frac{1}{g_{\text{dot}}(T)} \approx \frac{1}{g_l(T)} + \frac{1}{g_r(T)}. \quad (32)$$

The quantum mechanical interference effects in the dot are washed out for large enough temperatures. For lower temperatures the approximation Eq. (32) breaks down. Another temperature window where the result for the conductance takes a simple form is given by $|\Delta_a^{(\alpha)}(\varepsilon_\alpha)| \ll T \ll B/N_D$. If the resonance is at the chemical potential or much closer to it than T the conductance decays with temperature $\propto w_\alpha/T$. For the interacting case discussed in Sect. V the weight of the resonance w_α itself is temperature dependent which results in $G(T) \propto T^{\alpha_B-1}$.

The above arguments for weak hopping connections of the dot with the rest of the system can easily be generalized to the case of $\tilde{t}_a \approx 1$ but a large site impurity V_a at the site \tilde{j}_a . For $|V_l| \gg 1$ the site \tilde{j}_l can be "integrated out" using Eq. (17). This leads to a weak hopping $\tilde{t}_{j_{l-2}, j_l} = \tilde{t}_{j_{l-2}, j_{l-1}} \tilde{t}_l / V_l$ between the sites j_{l-2} and j_l .

The relations presented in this section play an important role for the interpretation of our fRG results for the transport through interacting quantum wires.

IV. THE FUNCTIONAL RENORMALIZATION GROUP AT $T > 0$

We now return to our Hamiltonian Eq. (1). Due to the presence of leads the direct calculation of the non-interacting propagator related to $H_{\text{kin}} + H_{\text{imp}}$ [see Eqs. (2) and (5)] requires the inversion of an infinite matrix. Using Eq. (17) it can be reduced to the inversion of an $N \times N$ matrix. The leads then provide an additional diagonal one-particle potential on sites 1 and N , depending on the Matsubara frequency ω_n ,

$$V_{j,j'}^{\text{lead}}(i\omega_n) = \frac{i\omega_n + \mu}{2} \left(1 - \sqrt{1 - \frac{4}{(i\omega_n + \mu)^2}} \right) \times \delta_{j,j'} (\delta_{1,j} + \delta_{N,j}). \quad (33)$$

Since the interaction is only non-vanishing on the bonds between the sites 1 to N the problem including the semi-infinite leads is this way reduced to the problem of an N -site chain. The chemical potential of the entire system in thermal equilibrium is denoted by $\mu(n, U, T)$.

To set up the fRG the projected non-interacting propagator G_0 is replaced by

$$G_0^\Lambda(i\omega_n) = \chi^\Lambda(\omega_n) G_0(i\omega_n) \quad (34)$$

with a function χ^Λ which is unity for $|\omega_n| \gg \Lambda$ and vanishes for $|\omega_n| \ll \Lambda$. At $T = 0$ we earlier considered $\chi^\Lambda(\omega) = \Theta(|\omega| - \Lambda)$.³⁴⁻³⁶ For technical reasons at $T > 0$ a smoother cutoff function, specified below, is more appropriate. We here choose to include the impurity part of the

Hamiltonian H_{imp} in G^0 . Earlier it was taken as a part of the self-energy.³⁶ At $T = 0$ both choices lead to the same results. By means of G_0^Λ the generating functional of the one-particle irreducible vertex functions for the Hamiltonian H becomes Λ dependent. Differentiating the functional with respect to Λ and expanding it in the external sources then leads to an exact infinite hierarchy of coupled flow equations for the vertex functions.³¹⁻³³ In practical applications this set of equations has to be truncated. As a first step we neglect the three-particle vertex which is small as long as the two-particle vertex Γ^Λ stays small which is the case for not-too-large U .³⁶ This approximation leads to a closed set of equations for Γ^Λ and the self-energy Σ^Λ given by

$$\frac{\partial}{\partial \Lambda} \Sigma^\Lambda(1', 1) = -\frac{1}{\beta} \sum_{2,2'} e^{i\omega_n 0^+} S^\Lambda(2, 2') \Gamma^\Lambda(1', 2'; 1, 2) \quad (35)$$

and

$$\begin{aligned} \frac{\partial}{\partial \Lambda} \Gamma^\Lambda(1', 2'; 1, 2) &= \frac{1}{\beta} \sum_{3,3'} \sum_{4,4'} G^\Lambda(3, 3') S^\Lambda(4, 4') \\ &\times \left[\Gamma^\Lambda(1', 2'; 3, 4) \Gamma^\Lambda(3', 4'; 1, 2) \right. \\ &- \Gamma^\Lambda(1', 4'; 1, 3) \Gamma^\Lambda(3', 2'; 4, 2) - (3 \leftrightarrow 4, 3' \leftrightarrow 4') \\ &\left. + \Gamma^\Lambda(2', 4'; 1, 3) \Gamma^\Lambda(3', 1'; 4, 2) + (3 \leftrightarrow 4, 3' \leftrightarrow 4') \right]. \end{aligned} \quad (36)$$

The labels 1, 2, etc., stand for the quantum numbers of the non-interacting one-particle basis and the Matsubara frequencies. The full propagator G^Λ is given by

$$G^\Lambda = [(G_0^\Lambda)^{-1} - \Sigma^\Lambda]^{-1} \quad (37)$$

and the so-called single-scale propagator S^Λ by

$$S^\Lambda = G^\Lambda \left[\frac{\partial}{\partial \Lambda} (G_0^\Lambda)^{-1} \right] G^\Lambda. \quad (38)$$

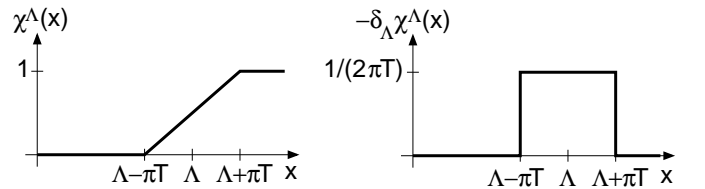


FIG. 2: The cutoff function $\chi^\Lambda(x)$ for fixed Λ and the negative of its derivative (with respect to Λ).

We choose the cutoff function

$$\chi^\Lambda(\omega_n) := \begin{cases} 0, & |\omega_n| \leq \Lambda - \pi T \\ \frac{1}{2} + \frac{|\omega_n| - \Lambda}{2\pi T}, & \Lambda - \pi T \leq |\omega_n| \leq \Lambda + \pi T \\ 1, & |\omega_n| \geq \Lambda + \pi T \end{cases}$$

with the accompanying derivative

$$-\frac{\partial}{\partial \Lambda} \chi^\Lambda(\omega_n) = \begin{cases} \frac{1}{2\pi T}, & \Lambda - \pi T \leq |\omega_n| \leq \Lambda + \pi T \\ 0, & \text{otherwise,} \end{cases}$$

where Λ starts at ∞ and goes down to 0. Both these functions are shown in Fig. 2. With this choice and for a fixed Λ a Matsubara sum involving the single-scale propagator Eq. (38) contains only the two terms with frequencies $\Lambda - \pi T < |\omega_n| < \Lambda + \pi T$. This reduces the numerical effort in solving the coupled differential equations for the self-energy and the two-particle vertex. With this cutoff function the right-hand side of the flow equation has a jump at every Matsubara frequency and is smooth in between, such that the flow can be integrated by standard routines.

To obtain a manageable set of equations even for large N we next introduce further approximations in the flow

equation of the two-particle vertex.³⁶ We are dealing with at most two local impurities. For large N such a small number of impurities does not significantly alter the flow of the effective interaction and we thus neglect the feedback of the bare impurity potential entering G_0^Λ on the flow of Γ^Λ . Self-energy effects on the flow of Γ^Λ are of order U^3 and are ignored. For the integration of Eq. (36) we furthermore consider a system with constant U on all bonds. The two-particle vertex is projected onto the Fermi points and parameterized by a nearest-neighbor interaction U^Λ . After taking the limit $N \rightarrow \infty$ the flow equation for U^Λ reads³⁶

$$\frac{\partial}{\partial \Lambda} U^\Lambda = h(\tilde{\omega}_n) (U^\Lambda)^2 \quad (39)$$

with

$$h(x) = -\frac{1}{2\pi} - \text{Re} \left[\frac{i}{2} (\mu_0 + ix) \sqrt{1 - \frac{4}{(\mu_0 + ix)^2}} \frac{3i\mu_0^4 - 10\mu_0^3 x - 12i\mu_0^2(x^2 + 1) + 6x^3\mu_0 + 18x\mu_0 + 6ix^2 + ix^4}{\pi(2\mu_0 + ix)(4 - \mu_0^2 + x^2 - 2ix\mu_0)^2} \right], \quad (40)$$

where $\tilde{\omega}_n$ stands for the fermionic Matsubara frequency closest to Λ , and $\mu_0 = -2 \cos k_F$. The above simplified flow equation yields not only the correct low energy asymptotics to second order in the renormalized vertex, but contains also all non-universal second order corrections to the vertex at $\pm k_F$ at higher energy scales.³⁶ In the case where the interaction depends on position, as an additional approximation we apply Eq. (39) locally for each bond. As long as the bulk part of the interacting wire is much larger than the contact regions this has a small effect.

Because of the above approximations the self-energy is a frequency-independent tridiagonal matrix in real space: only $\Sigma_{j,j}$ and $\Sigma_{j,j\pm 1}$ are non-zero. In the exact solution a frequency dependence of Σ is generated to order U^2 (bulk TLL behavior), which shows that in the approximation for the self-energy terms of order U^2 are only partly included. For the flow of the T - and N -dependent self-energy we obtain

$$\begin{aligned} \frac{\partial}{\partial \Lambda} \Sigma_{j,j}^\Lambda &= -\frac{1}{2\pi} \sum_{|\omega_n| \approx \Lambda} \sum_{r=\pm 1} U_{j,j+r}^\Lambda \left[\frac{1}{Q(i\omega_n) - \chi^\Lambda(\omega_n)\Sigma^\Lambda} \right. \\ &\quad \left. \times Q(i\omega_n) \frac{1}{Q(i\omega_n) - \chi^\Lambda(\omega_n)\Sigma^\Lambda} \right]_{j+r,j+r} \\ \frac{\partial}{\partial \Lambda} \Sigma_{j,j\pm 1}^\Lambda &= \frac{1}{2\pi} \sum_{|\omega_n| \approx \Lambda} U_{j,j\pm 1}^\Lambda \left[\frac{1}{Q(i\omega_n) - \chi^\Lambda(\omega_n)\Sigma^\Lambda} \right. \\ &\quad \left. \times Q(i\omega_n) \frac{1}{Q(i\omega_n) - \chi^\Lambda(\omega_n)\Sigma^\Lambda} \right]_{j,j\pm 1}, \end{aligned}$$

where $|\omega_n| \approx \Lambda$ stands for taking the positive as well as negative frequency with absolute value closest to Λ , and $j, j\pm 1 \in [1, N]$. The matrix Q is the inverse of the cutoff-independent, projected, and non-interacting propagator $Q = (G_0)^{-1}$.

The initial condition of the self-energy at $\Lambda = \infty$ is given by

$$\begin{aligned} \Sigma_{j,j}^\infty &= -\nu(n, U) (U_{j-1,j} + U_{j,j+1}) \\ \Sigma_{j,j\pm 1}^\infty &= 0, \end{aligned}$$

and the one of the flowing nearest-neighbor interaction by $U^\infty = U$. In a numerical solution the flow starts at a large finite initial cutoff Λ_0 . One has to take into account that, due to the slow decay of the right-hand side of the flow equation for Σ^Λ , the integration from $\Lambda = \infty$ to $\Lambda = \Lambda_0$ yields a contribution which does not vanish for $\Lambda_0 \rightarrow \infty$, but rather tends to a finite constant.³⁶ The resulting initial condition at $\Lambda = \Lambda_0 \rightarrow \infty$ reads

$$\begin{aligned} \Sigma_{j,j}^{\Lambda_0} &= [1/2 - \nu(n, U)] (U_{j-1,j} + U_{j,j+1}) \\ \Sigma_{j,j\pm 1}^{\Lambda_0} &= 0. \end{aligned}$$

The right-hand side of Eq. (39) tends to zero fast enough so that no such additional contribution is built up for the flowing interaction and $U^{\Lambda_0} = U$.

Neglecting the leads, at $T = 0$, and in the limit of a single weak or strong impurity the coupled differential equations (39) and (41) can be solved analytically.³⁵ The results are consistent with what is expected from the

LSGM. For general parameters we solve the flow equations numerically. We have developed an algorithm⁵⁶ which for $T > 0$ approximately scales with N/T . For finite T systems of 10^4 lattice sites are considered, roughly corresponding to the length of quantum wires accessible to transport experiments. Since the interacting wire consists of N lattice sites the energy scale

$$\delta_N = \frac{\pi v_F}{N} \quad (42)$$

forms a lower bound for any temperature scaling of the conductance with an interaction dependent exponent (see Sect. V) and $G(T)$ quickly saturates for $T \lesssim \delta_N$. Therefore only temperatures of the order of the band width down to $T = 10^{-4}$ are relevant and have been studied. The Fermi velocity is given by $v_F = 2 \sin k_F$, with the Fermi momentum $k_F = n\pi$. We note that the saturation of Σ^Λ for $\Lambda \lesssim T$ or $\Lambda \lesssim \delta_N$ sets in “automatically”, in contrast to more intuitive renormalization group schemes in which the flow of the considered quantities is stopped “by hand” by replacing $\Lambda \rightarrow T$ or $\Lambda \rightarrow \delta_N$, respectively.^{6,7,9,24,25}

At the end of the flow ($\Lambda = 0$), $\Sigma^{\Lambda=0}$ presents an approximation for the exact self-energy and will be denoted by Σ in what follows. The fRG is set up in the grand canonical ensemble with fixed chemical potential μ . As we want to compare our results with those obtained for the LSGM considering the canonical ensemble with fixed density n we first determine the parameter $\nu(n, U)$ such that at $T = 0$ the density on the sites 1 to N acquires the desired value n . In a second step the global chemical potential $\mu(n, U, T)$ is determined such that the density of the entire system (interacting wire and leads) remains n for all T . Due to particle-hole symmetry in the half-filled case we have $\nu(1/2, U) = 1/2$ and $\mu(1/2, U, T) = 0$.

Typical results of the N -dependent $\Sigma_{j,j}$ and $\Sigma_{j,j+1}$ at $T = 0$ for a single impurity located at site j_0 and $U > 0$ were presented in Figs. 5 and 6 of Ref. 36. Both matrix elements show long-ranged spatial oscillations induced by the impurity with an amplitude which asymptotically decays as $1/|j - j_0|$.³⁶ For finite T this power-law decay of the self-energy induced by a single impurity is cut off at a scale $\propto 1/T$ beyond which the oscillatory part of $\Sigma_{j,j}$ and $\Sigma_{j,j+1}$ decays exponentially. This is exemplified in Fig. 3 in which $|\Delta\Sigma_{j,j+1}| = |\Sigma_{j,j+1} - \bar{\Sigma}_o|$ is shown for different T and as a function of $j - j_0$. The average value of $\Sigma_{j,j+1}$ away from the impurity site, which is related to the interaction-induced broadening of the band, is denoted by $\bar{\Sigma}_o$. In the left panel of Fig. 3, $|\Delta\Sigma_{j,j+1}|$ is shown on a log-log scale where straight lines are power-laws, while in the right panel it is presented on a linear-log scale where straight lines represent an exponential decay. The self-energy was calculated for the case of a single hopping impurity with $t' = 0.1$ located in the middle of the interacting wire with $N = 10^4$ sites. The other parameters are $U = 1$ and $n = 1/2$. For a hopping impurity and at half filling the diagonal part of the self-energy $\Sigma_{j,j}$ vanishes.

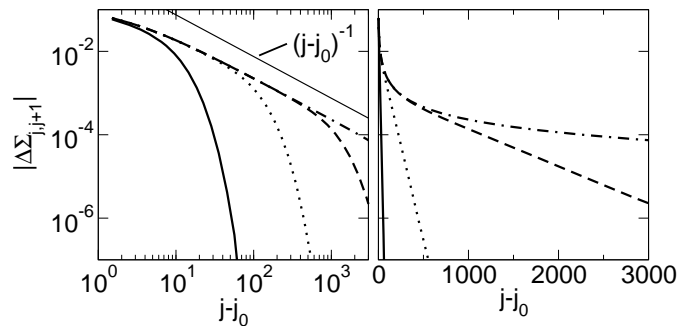


FIG. 3: Decay of the oscillatory part of the off-diagonal matrix element of the self-energy away from a single hopping impurity at bond $j_0, j_0 + 1$. Results for $t' = 0.1$, $j_0 = 5000$, $N = 10^4$, $U = 1$, $n = 1/2$ and different temperatures $T = 10^{-1}$ (solid line), $T = 10^{-2}$ (dotted line), $T = 10^{-3}$ (dashed line), and $T = 10^{-4}$ (dashed-dotted line) are presented. The left panel shows the data on a log-log scale, the right panel on a linear-log scale. For comparison the left panel contains a power-law $(j - j_0)^{-1}$ (thin solid line).

From Σ we obtain an approximation for the conductance $G(T)$ through our interacting system. We use the fact that it is consistent to neglect vertex corrections to the Landauer-Büttiker formula when the approximate self-energy is frequency independent.⁵⁷ This is the case in our fRG scheme as discussed in the Appendix. Therefore using Eq. (16) does not imply any further approximation. To obtain $G(T)$ we have to calculate the effective, T - and δ_N -dependent transmission $|t(\varepsilon, T, \delta_N)|^2$ (where the dependences on ε , T , and δ_N are from now on written explicitly) which is expressed in terms of the one-particle Green function between sites 1 and N [see Eq. (15)] and can be calculated by inverting the tridiagonal matrix $Q - \Sigma$. This way we have reduced the many-body problem to a single-particle scattering problem off an effective impurity potential on the sites 1 to N given by the T - and δ_N -dependent self-energy. For the detailed understanding of our findings for the single- and double-barrier case we use the one-particle scattering theory results derived in Sect. III.

A comparison of the fRG results for a single impurity at $T = 0$ to accurate DMRG results and exact scaling properties shows that the error due to our various approximations is small for interactions such that $1/2 \leq K \leq 1$.^{36,38} As we discuss next, the same holds at finite T .

V. RESULTS

A. Single impurity

In this section we report our results for transport through a single impurity, and later through a double barrier. In the single impurity case we mainly consider site impurities; we have obtained similar results for hopping impurities. We first consider impurities placed suf-

ficiently away from the contact regions and then briefly discuss the dependence of the conductance on the impurity position j_0 .

Fig. 4 shows typical fRG results for the T dependence of the conductance in the case of a single site impurity of strength V . The parameters are $U = 0.5$, $n = 1/2$, and $N = 10^4$. For $T \geq B$ all curves show a $1/T$ scaling. For these temperatures the derivative of the Fermi function in Eq. (16) only varies very weakly with ε for the relevant energies $-B/2 \leq \varepsilon \leq B/2$ but decreases with increasing temperature as $1/T$. At the same time the integral over the band energies of $|t(\varepsilon, T, \delta_N)|^2$ is only weakly T -dependent leading to the observed $1/T$ behavior. For a strong impurity $V = 10$ and $\delta_N \leq T \ll B$, $G(T)$ nicely follows a power-law with an exponent $\beta_s(U, n)$ indicated in Fig. 4 by the dotted line. More specifically we find for all U and n that power-law scaling does not set in before $T \gtrsim B/40$. It holds down to $T \approx \delta_N/2$ ($\approx 3 \cdot 10^{-4}$ for $N = 10^4$) beyond which the conductance saturates. The exact value of this lower bound depends on the impurity position j_0 (see below).¹⁵ We here consider $j_0 \approx N/2$. For an intermediate impurity $V = 1$ the slope of the data (on a log-log scale) tends towards β_s but is still significantly away from it when saturation sets in at $\delta_N/2$. The slow change of the slope seen in Fig. 4 is a general feature of intermediate V . This observation is of relevance for the analysis of noisy experimental data usually restricted to temperatures within one to two orders of magnitude.^{42,43} Under these conditions a transient regime might easily incorrectly be identified as the asymptotic power-law regime leading to an exponent which is too small. For a weak impurity $G(T)$ stays very close to e^2/h for all $T \ll B$.

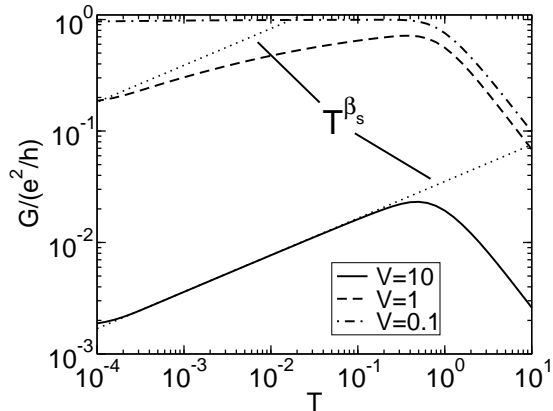


FIG. 4: Temperature dependence of the conductance for a single site impurity with different V as indicated in the legend and $U = 0.5$, $n = 1/2$, $N = 10^4$. The dotted line shows a power-law with an exponent β_s obtained from fitting the $V = 10$ data.

In Fig. 5 the U -dependence of the strong-impurity exponent β_s is shown for $n = 1/2$ (circles) and $n = 1/4$ (squares). We also present results for $U < 0$, where $G(T)$ increases for decreasing T and $\beta_s < 0$. In this

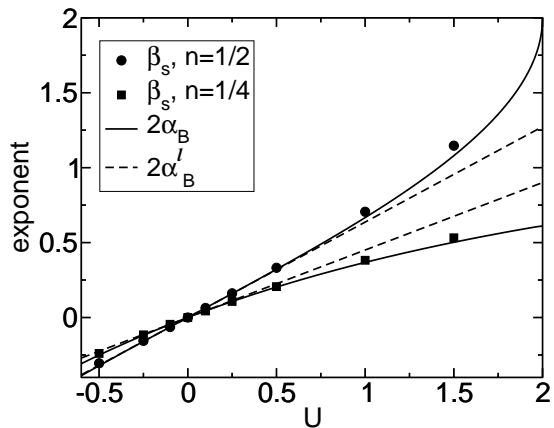


FIG. 5: Dependence of the strong-impurity exponent β_s on the interaction U . For comparison the LSGM prediction $2\alpha_B$ (solid line) and the leading order (in U) result $2\alpha_B^l$ (dashed line) are shown.

case $G(T) \propto T^{\beta_s}$ does not present the asymptotic low-energy behavior since for $T \rightarrow 0$, $G(T)$ is tending towards e^2/h . The larger $|U|$, the faster $G(T)$ increases. At the same time the temperature regime over which a power-law exponent can be read off shrinks even if V is chosen to be very large. An exponent can be reliably read off for $U \geq -0.5$ only. From the studies of the LSGM^{6,10} we expect that the strong-impurity exponent is $2\alpha_B = 2(1/K - 1)$. For $n = 1/2$, K is given in Eq. (10) while away from half filling it can be calculated solving the Bethe ansatz integral equations numerically.⁵⁰ For comparison, $2\alpha_B$ (solid line) and the leading- U behavior

$$2\alpha_B^l = 2 \frac{2U(1 - \cos[2k_F])}{2\pi v_F} \quad (43)$$

(dashed line) are presented in Fig. 5. The exponent β_s turns out to be at least correct to leading order in U . Furthermore, even for intermediate $U \gtrsim 1.5$, it is still very close to $2\alpha_B$ in contrast to the leading-order contribution $2\alpha_B^l$.

For weak impurities $G(T)$ is predicted to follow a power-law scaling $1 - G(T)/(e^2/h) \propto T^{2(K-1)}$ which holds as long as the correction to perfect conductance stays small.^{6,10} For $K - 1 > 0$, i.e. $U < 0$, this scaling presents the asymptotic low-energy behavior. In Fig. 6, $1 - G(T)/(e^2/h)$ is shown for $V = 0.01$, $n = 1/2$, $N = 10^4$, and different U . We can read off an exponent $\beta_w(U, n)$. In Fig. 7, β_w for $n = 1/2$ and $n = 1/4$ is compared to $2(K - 1)$ and the leading-order term $-2\alpha_B^l$. Note that to leading order $2\alpha_B = 2(1 - K)$, which will become important in the comparison of the fRG to the “leading-log” method. Our weak-impurity exponent β_w agrees to first order in U with $2(K - 1)$, but is closer to the exact result than $-2\alpha_B^l$.

In the solution of the LSGM the strong- and weak-impurity exponents characterizing the scaling of G can both be expressed in terms of K . Identifying $\beta_s =$

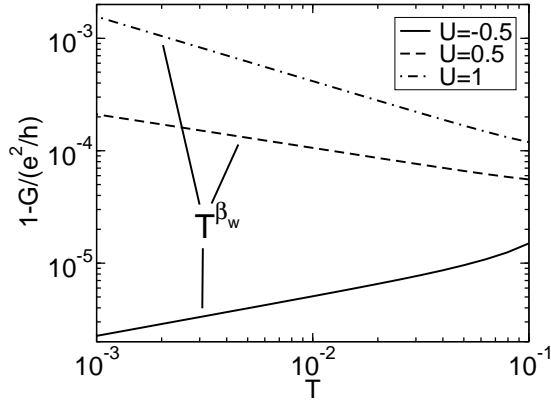


FIG. 6: Weak-impurity behavior of $1 - G(T)/(e^2/h)$ for $V = 0.01$, $n = 1/2$, $N = 10^4$ and different U as indicated in the legend.

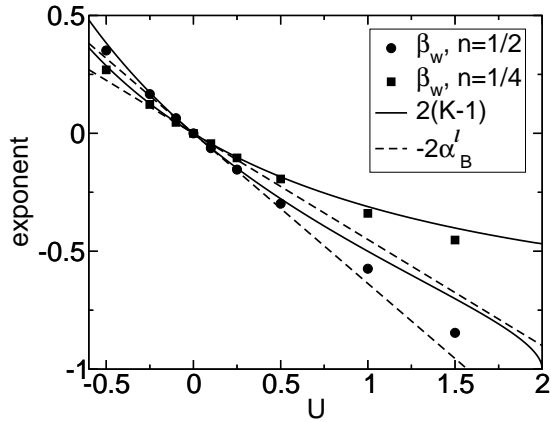


FIG. 7: Dependence of the weak-impurity exponent β_w on the interaction U . For comparison the LSGM prediction $2(K-1)$ (solid line) and the leading order (in U) result $-2\alpha_B^l$ (dashed line) are shown.

$2(1/K_s - 1)$ and $\beta_w = 2(K_w - 1)$ we obtain two fRG approximations K_s and K_w for K . In Fig. 8 the relative error of the fRG approximations to the exact TLL parameter $\Delta K/K = |K - K_{s/w}|/K$ is presented for $n = 1/2$ and $n = 1/4$. From the figure it is apparent that $\Delta K \propto U^2$. In our approximation scheme terms of order U^2 are only partially included³⁶ and we thus cannot expect agreement to higher order. The error $\Delta K/K$ depends on n . The half-filled case exhibits the largest deviation from the exact result. This can be understood from the flow of U^Λ . For fixed $U > 0$ as a function of n , $(U^{\Lambda=0} - U)/U$ becomes maximal at $n = 1/2$, where the nearest-neighbor interaction increases by a few 10 percent (for an example at $T = 0$ and $U = 1$ see Fig. 4 of Ref. 36). In contrast for smaller fillings, e.g. $n = 1/4$, U^Λ even decreases during the flow. This explains why our weak coupling method works particularly well for small fillings. The two approximations K_s and K_w differ to order U^2 which shows that within our approach the TLL relation between the strong- and weak-impurity exponents

is only fulfilled approximately.

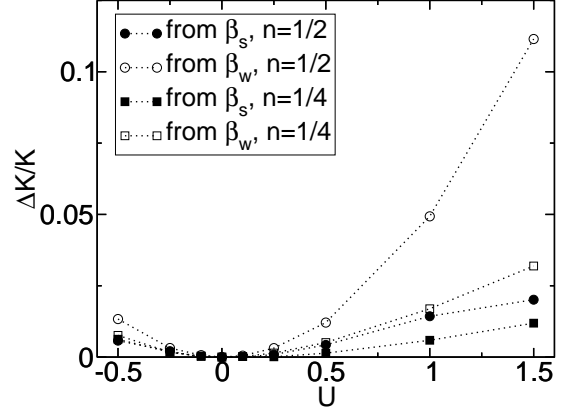


FIG. 8: Relative error of the fRG approximations for the TLL parameter from the strong- β_s and weak- β_w impurity exponents at $n = 1/2$ and $n = 1/4$.

In the LSGM with repulsive interaction even a weak bare impurity induces a power-law suppression of G with exponent $2\alpha_B$ in the limit where all energy scales are sent to zero. For weak bare impurities and $1/2 \leq K < 1$, the crossover scale between weak- and strong-impurity behavior goes as $V^{1/(1-K)}$ and becomes very small.^{6,8,10} For the lattice model considered here we have observed a similarly small scale.³⁸ As a consequence, even for the fairly large system size of $N = 10^4$ sites and the large range of temperatures we can treat, it is impossible to directly demonstrate the full crossover for a single set of parameters. In the LSGM it can be shown indirectly using a one-parameter scaling ansatz

$$G = \frac{e^2}{h} \tilde{G}_K(x), \quad x = [T/T_0(U, n, V)]^{K-1} \quad (44)$$

with a non-universal scale $T_0(U, n, V)$.^{6,8,10} For appropriately chosen T_0 the $G(T)$ curves for different V (but fixed K) can be collapsed onto the K -dependent scaling function $\tilde{G}_K(x)$. It has the limiting behavior $\tilde{G}_K(x) \propto 1 - x^2$ for $x \rightarrow 0$ and $\tilde{G}_K(x) \propto x^{-2/K}$ for $x \rightarrow \infty$. We earlier demonstrated one-parameter scaling for the microscopic lattice model considered within our approximation scheme replacing T in the above ansatz Eq. (44) by δ_N .³⁸ To set up the scaling we have to decide whether we take K_s or K_w in the definition of the variable x . For a comparison to the analytically known $K = 1/2$ scaling function of the LSGM it is advantageous to use K_s , since for the corresponding U [$U = 2$ for $n = 1/2$; see Eq. (10)] K_s is much closer to the exact K than K_w . (see Fig. 8). This is what we did in Ref. 38. This choice leads to a small deviation from the $1 - x^2$ behavior at small x . For small U the difference in the approximate TLL parameters is small and we here use K_w instead. In the limit $x \rightarrow 0$ it implies an exact $1 - x^2$ behavior of the fRG approximation for the scaling function. A one-parameter scaling plot is shown in Fig. 9. The

different symbols stand for different $V \in [0.01, 30]$. For each V , $G(T)$ was calculated for several $T \in [10^{-3}, 10^{-1}]$. The open symbols represent results obtained at half filling for $U = 0.5$ which gives $K_w = 0.85$. The same K_w we find for quarter-filling and $U = 0.851$. Data for the latter parameters are shown as filled symbols. The collapse of the results for $n = 1/2$ and $n = 1/4$ exemplifies that the scaling function depends on U and n only via the TLL parameter K as predicted for the LSGM. It is very remarkable that our exponent $2\beta_s/\beta_w$ of the large x -behavior agrees to leading order with the corresponding exponent $-2/K$ of the LSGM. This is a significantly stronger result than the observation that β_s and $2\alpha_B$ as well as β_w and $2(K - 1)$ agree to order U . Considering site (hopping) impurities which are extended over more than one site (bond) as well as impurities which are given by a combination of modified on-site energies and hopping matrix elements we have verified that \tilde{G}_K is also independent of the details of the local impurity.

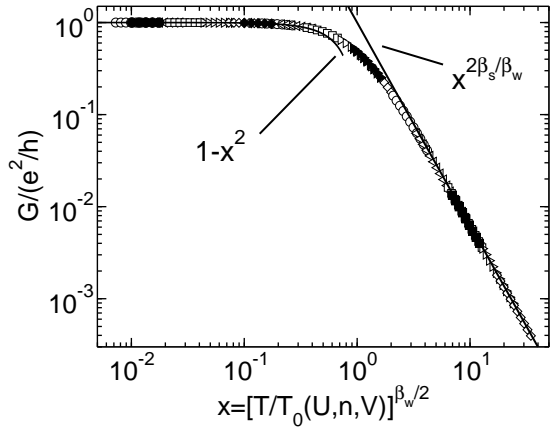


FIG. 9: One-parameter scaling plot of the conductance. Open symbols represent results obtained for $U = 0.5$, $n = 1/2$, and different T and V , while filled symbols were calculated for $U = 0.851$, $n = 1/4$. Both pairs of U and n lead to the same $K_w = 0.85$. The solid lines indicate the asymptotic behavior for small and large x .

A comparison of the results presented here for fixed δ_N and varying T and the results of Ref. 38 obtained for $T = 0$ and different δ_N shows that in the single-impurity case and for smooth contacts δ_N and T present equivalent scaling variables. In alternative RG schemes this equivalence is instead assumed. Note that the equivalence no longer holds if either non-perfect contacts^{38,58} or resonant tunneling is considered (for the latter, see below).

In Ref. 9 an alternative fermionic RG method was introduced to study an effective low-energy model with a single barrier in the limit of weak interaction. In this approach an RG equation is set up to resum the “leading-log” divergences of the effective transmission at the chemical potential. The results obtained using the “leading-log” method only partly agree to ours. While in our approach the one-parameter scaling function depends on

K and the exponent $-2/K$ of the large x -behavior is reproduced correctly to order U , the one-parameter scaling function of the “leading-log” approach turns out to be the non-interacting ($K = 1$) function independently of the interaction strength chosen.⁹ This method thus does not capture all leading-order interaction effects.

This shortcoming of the “leading-log” method can be traced back to the analytical form of the effective transmission at scale Λ

$$|t^\Lambda|^2 = \frac{|t_0|^2 |\Lambda/\lambda_0|^{2\alpha_B^l}}{|r_0|^2 + |t_0|^2 |\Lambda/\lambda_0|^{2\alpha_B^l}} \quad (45)$$

as it follows from the RG equations.⁹ The impurity parameters (height and width) enter via the non-interacting transmission and reflection probabilities at the chemical potential $|t_0|^2$ and $|r_0|^2$, and λ_0 denotes a non-universal energy scale. As above the exponent α_B^l stands for the leading-order term of $\alpha_B = 1/K - 1$. This equation is derived under the assumption that all energy scales, i.e. T , δ_N , and the energy of the incoming particle ε (measured relative to the chemical potential) are set to zero. The dependence on T , δ_N , or ε is then determined by replacing Λ by one of these variables. For $T = 0$, at the chemical potential, but for a finite system this gives

$$|t(\delta_N)|^2 = \frac{|t_0|^2 (\delta_N/\delta_0)^{2\alpha_B^l}}{|r_0|^2 + |t_0|^2 (\delta_N/\delta_0)^{2\alpha_B^l}}, \quad (46)$$

with the non-universal scale δ_0 . Applying Eq. (16), which for $T = 0$ reduces to $G = e^2 |t(\mu)|^2/h$, and introducing $x = |r_0/t_0| (\delta_N/\delta_0)^{-\alpha_B^l}$, where $-\alpha_B^l$ is the leading-order term of $K - 1$, the scaling function of the conductance turns out to be the non-interacting one, $\tilde{G}_{K=1} = 1/(1 + x^2)$. Eq. (46) can be compared to our Eq. (24) which applies to the situation of a single site impurity ($V_g = V$). Because of the above-mentioned equivalence of the T and δ_N scaling it is sufficient to consider $T = 0$ and the length of the interacting wire as the variable. Without loss of generality we here focus on $n = 1/2$ with $\mu = 0$. For $t_l = \tilde{t}_r$, $T = 0$, and at the chemical potential, i.e. for $\varepsilon = 0$, Eq. (24) reads

$$|t(0, 0, \delta_N)|^2 = \frac{4\Delta^2(0, 0, \delta_N)}{\left[\tilde{V} + 2\Omega(0, 0, \delta_N)\right]^2 + 4\Delta^2(0, 0, \delta_N)}. \quad (47)$$

Because of the left-right symmetry we here and in the following suppress the index l/r . During the flow the potential V on the impurity site gets renormalized. At $\Lambda = 0$ it is denoted by \tilde{V} . Eq. (47) holds for a more general impurity in which also the hopping amplitude $t_l = t_r$ [see the discussion following Eq. (9)] to the left and right of the lattice site with onsite energy V is different from one.⁵⁹ Δ and Ω can be obtained numerically from the self-energy at $\Lambda = 0$ as explained in Sect. III. For $V \rightarrow 0$, which implies $\tilde{V} \rightarrow 0$ because of the particle-hole-symmetry for $V = 0$, and sufficiently large N we

find

$$\tilde{V} + 2\Omega(0, 0, \delta_N) \propto \delta_N^{\beta_w/2}, \quad \Delta(0, 0, \delta_N) = \text{const.} \quad (48)$$

while for $V \gg B$

$$\tilde{V} + 2\Omega(0, 0, \delta_N) = \text{const.}, \quad \Delta(0, 0, \delta_N) = \delta_N^{\beta_s/2}. \quad (49)$$

Instead of the one exponent α_B^l of the “leading-log” approach we obtain two different exponents characterizing the weak- and strong-impurity limits. This leads to an interaction-dependent scaling function with a large x scaling exponent which is correct to leading order in U . In contrast to Eq. (46) the analytical form Eq. (47) allows for two different sources of an N -dependence of the effective transmission and the conductance. We thus conclude that reducing the number of flowing coupling constants to a single one — the effective transmission at the chemical potential — leads to an analytic form of the conductance which is too restricted to cover all important leading-order interaction effects. This shows that our fRG approach goes beyond the “leading-log” method.

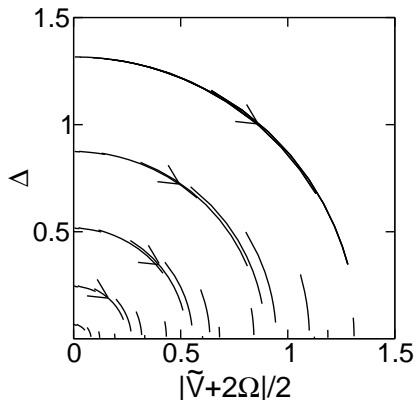


FIG. 10: Flow diagram of the conductance in the plane defined by the real and imaginary part of the auxiliary Green function. The direction of the flow for $\delta_N \rightarrow 0$ and $U > 0$ is indicated by the arrows. For $U < 0$ it is reversed. The axes are lines of fixed points. Δ -axis: line of “perfect chain” fixed points with $G = e^2/h$. $(\tilde{V} + 2\Omega)$ -axis: line of “open chain” fixed points with $G = 0$.

Eq. (47) can be used to further visualize the scaling of the conductance. Within our approximation the conductance can be expressed in terms of the two scale- and parameter-dependent functions $(\tilde{V} + 2\Omega)/2$ and $\Delta \geq 0$. Fig. 10 shows a parameter plot in the $([\tilde{V} + 2\Omega]/2, \Delta)$ plane obtained at $\varepsilon = T = 0$ and for varying N . Each curve was calculated for a fixed V and $t_l = t_r$ at $U = 1$ and half filling. A similar plot can be obtained for a large fixed N calculating $(\tilde{V} + 2\Omega)/2$ and Δ for different $\Lambda > 0$ considering Σ^Λ as an effective scattering potential. With increasing N , i.e. decreasing energy scale, the “flow” approximately follows a section of a circle centered around the origin, with a radius which depends on the initial impurity parameters. For $U > 0$ the “flow” is clock-wise.

For attractive interaction the direction is reversed. The axis with $(\tilde{V} + 2\Omega)/2 = 0$ can be considered as a line of “perfect-chain” fixed points with $|t|^2 = 1$, while the axis with $\Delta = 0$ represents the line of “open-chain” fixed points with $|t|^2 = 0$. In accordance with Eqs. (48) and (49), close to the two lines of fixed points the “flow” is perpendicular to the axis.

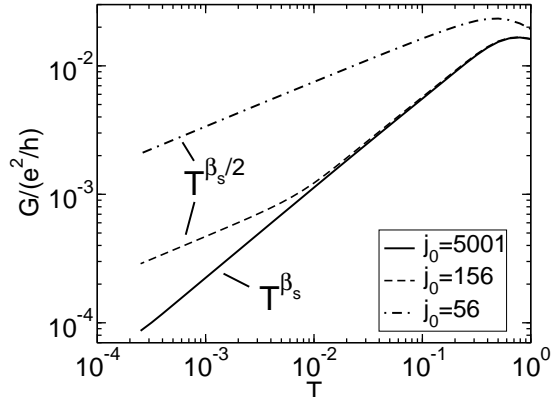


FIG. 11: The conductance $G(T)$ for a site impurity with $V = 10$, $U = 1$, $n = 1/2$, $N = 10^4 + 1$, and different impurity positions j_0 .

The above results are generic as long as the impurity is placed sufficiently away from the contact regions. A richer behavior is found if the impurity is positioned closer to the smooth contacts. Because of symmetry we only have to consider the case in which the impurity is moved towards the left contact. Then the scale

$$\delta_{j_0} = \frac{\pi v_F}{j_0} \quad (50)$$

becomes important.¹⁵ It sets the lower bound for the power-law scaling with the exponents discussed above. For $T \approx \delta_{j_0}$ we find a crossover to a power-law scaling with different exponents. This is exemplified in Fig. 11 for a strong impurity with $V = 10$, $N = 10^4 + 1$, $U = 1$ and three impurity positions $j_0 = 5001$ (solid line), 156 (dashed line), 56 (dashed-dotted line). For $j_0 = 156$ at $T \approx \delta_{j_0}$ the scaling with exponent β_s crosses over to a scaling with exponent $\beta_s/2$. This coincides with the prediction obtained within a field theoretical model where the exponent $2\alpha_B$ crosses over to half its value α_B .¹⁵ For impurity positions in the contact region, i.e. $j_0 = 56$, we only observe the exponent $\beta_s/2$ that describes the tunneling between the non-interacting leads and the TLL. The curve for $j_0 = 56$ does not follow the other two curves even at higher temperatures as compared to the bulk value the interaction at j_0 is reduced by a factor of two.

Similar behavior is found for the scaling of $1 - G(T)/(e^2/h)$ in the limit of a weak impurity. In this case the exponent predicted for $\delta_N < T < \delta_{j_0}$ is $2(K - 1)/(K + 1)$ and is thus different from half the exponent $2(K - 1)$ found for $\delta_{j_0} < T \ll B$.¹⁵ The exponent we find agrees to leading order in U with this

prediction. We note that even though $\beta_w/2$ agrees with $2(K-1)/(K+1)$ to order U our exponent in this regime is different from $\beta_w/2$.

B. Resonant tunneling

In this section we only investigate repulsive interactions $U > 0$ and focus on $n = 1/2$, with $\mu = 0$, as the results for other fillings do not differ qualitatively. We furthermore only consider situation in which the quantum dot is placed sufficiently away from the contact regions.

1. $T = 0$

We start our investigation of resonant tunneling considering $T = 0$. Fig. 12 shows typical results for the gate-voltage V_g dependence of the conductance for symmetric barriers. The quantum dot contains $N_D = 6$ sites and is separated from the rest of the interacting wire by two site impurities of intermediate height $V_{l/r} = 2$. In the figure the N -independent $U = 0$ result (dashed-dotted line) is compared to the conductance of fRG calculations with $U = 1$ for two different N . For not-too-weak barriers the number of perfect resonances (with peak conductance e^2/h) at positions V_g^r coincides with the number N_D of lattice sites which form the dot. For intermediate barriers and $U = 0$ the peaks still overlap. For increasing $V_{l/r}$ the width of each peak decreases until well-separated resonances are formed. Also for $U > 0$, G shows perfect resonances with peak conductance $G_p = e^2/h$. This behavior can be understood from Eq. (27), which for $U > 0$ and sufficiently large N can be used even for weak to intermediate barriers as the resonance peaks do no longer overlap. This was the necessary condition for the derivation of Eq. (27). At V_g^r we find $\varepsilon_\alpha + 2\Omega^{(\alpha)}(0, 0, \delta_N) = 0$. Regardless of the N -dependence of $\Delta^{(\alpha)}(0, 0, \delta_N)$ this leads to $|t(0, 0, \delta_N)|^2 = 1$. At $T = 0$ only $\varepsilon = 0$ contributes in the Landauer-Büttiker formula (16), leading to $G = e^2/h$. Remarkably, $\Delta^{(\alpha)}(0, 0, \delta_N)$ at V_g^r does not follow the scaling $\delta_N^{\beta_s/2}$ of the spectral weight close to a single impurity⁶ but instead saturates at small δ_N . The imaginary part of the exact Green function, which can be calculated from the auxiliary Green function using Eq. (28), behaves similarly. Increasing U at fixed N reduces the overlap between the resonances by increasing the energy difference between the peaks but even more importantly by reducing the width of each peak. The half-width σ depends on N . We find that the width of all peaks scales to zero as

$$\sigma \propto \delta_N^{-\beta_w/2} \quad (51)$$

with the weak-single-impurity exponent β_w as discussed in the last section. For $N \rightarrow \infty$ the resonances are thus

infinitely sharp. It is important to note that for all parameter sets tested we found agreement between twice the scaling exponent of σ at $T = 0$ and the weak-single-impurity exponent up to our numerical accuracy. The difference of σ for the different resonance peaks at a fixed N (see Fig. 12) is a band effect. Off resonance, G vanishes as

$$G \propto \delta_N^{\beta_s}, \quad (52)$$

with the strong-single-impurity exponent β_s (again up to the numerical accuracy). Using Eq. (27) this behavior can be traced back to a $\Delta^{(\alpha)}(0, 0, \delta_N) \propto \delta_N^{\beta_s/2}$ scaling while $\varepsilon_\alpha + 2\Omega^{(\alpha)}(0, 0, \delta_N)$ goes to a constant different from 0. Off resonance the double barrier acts as a single impurity of strength $\Delta V_g = V_g - V_g^r$.⁶ With this insight and using the one-parameter scaling ansatz Eq. (44) the N -dependence of σ , Eq. (51) can be explained as follows: For small $|\Delta V_g|$ the non-universal scale (here δ_0) goes as $|\Delta V_g|^{1/(1-K)}$. With $\tilde{G}_K(x_{1/2}) = 1/2$ this leads to $x_{1/2} = c\delta_N^{K-1} |\Delta V_g^{(1/2)}|$, with a ΔV_g -independent constant c . We thus find $\sigma = 2|\Delta V_g^{(1/2)}| \propto \delta_N^{1-K}$ which agrees with Eq. (51) to leading order in U .

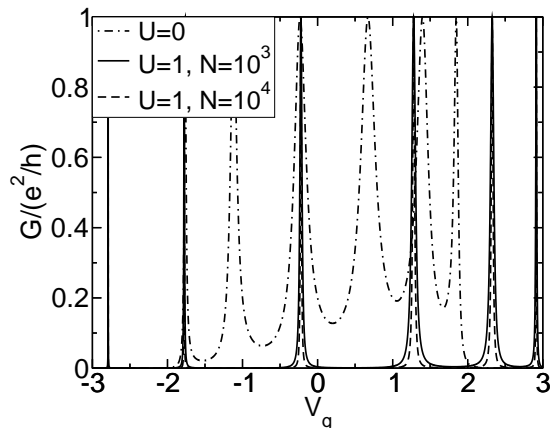


FIG. 12: Gate-voltage dependence of the conductance for a symmetric double barrier at $T = 0$. The parameters are $N_D = 6$ and $V_{l/r} = 2$.

For asymmetric barriers and $U = 0$ the conductance still displays resonances but with peak values G_p which are smaller than e^2/h . The same holds for $U > 0$ as is shown in Fig. 13 for hopping barriers with $t_l = 0.1$, $t_r = 0.3$, $U = 0.5$, and $N_D = 10$. We set the interaction across the barrier bonds to 0. The number of resonance peaks is N_D . Here we only show a single peak. For hopping impurities as barriers, G is symmetric around $V_g = 0$ (for $n = 1/2$). With increasing U and for fixed N , G_p decreases. The same holds for fixed U and increasing N . For sufficiently large N we find that Eq. (52) holds for the off- and on-resonance scaling, i.e. on small scales also at V_g^r an asymmetric double barrier acts as a single impurity. As a consequence for

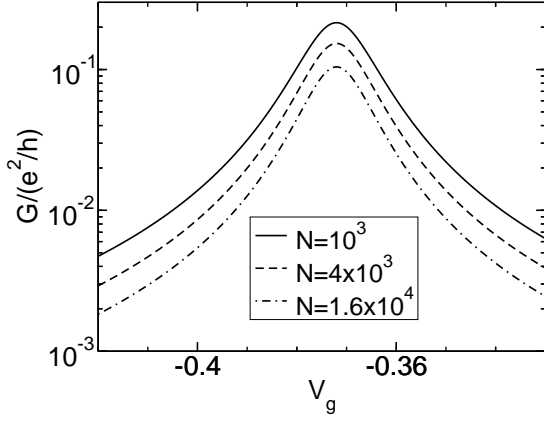


FIG. 13: Gate voltage dependence of the conductance for an asymmetric double barrier at $T = 0$. The parameters are $U = 0.5$, $N_D = 10$, $t_l = 0.1$, and $t_r = 0.3$. Only gate voltages close to V_g^r are shown. Note the linear-log scale.

$N \rightarrow \infty$ the half-width σ of the peaks approaches a constant. Again Eq. (27) can be used to further analyze G . At V_g^r , $\varepsilon_\alpha + \Omega_l^{(\alpha)}(0, 0, \delta_N) + \Omega_r^{(\alpha)}(0, 0, \delta_N) = 0$. For $t_r < t_l < 1$ and $\delta_N \rightarrow 0$, $\Delta_r(0, 0, \delta_N)$ vanishes as $\delta_N^{\beta_s/2}$ while $\Delta_l(0, 0, \delta_N)$ increases as $\delta_N^{-\beta_s/2}$. These results combine to Eq. (52). Applying Eq. (28) one can show that in contrast to the asymmetric behavior of the imaginary part $\Delta_{l/r}$ of the auxiliary Green function, the spectral function of the exact Green function on the sites to the right and the left of the barriers both scale to zero as $\delta_N^{\beta_s/2}$. The off-resonance behavior can be explained similarly as for symmetric barriers: $\Delta_{l/r}(0, 0, \delta_N) \propto \delta_N^{\beta_s/2}$ while $\varepsilon_\alpha + \Omega_l^{(\alpha)}(0, 0, \delta_N) + \Omega_r^{(\alpha)}(0, 0, \delta_N)$ goes to a constant different from 0. We obtain all the above results for both hopping and site impurities as barriers.

Within an extension of the LSGM to the two-barrier case resonant tunneling on asymptotically small scales has been discussed in Ref. 6. The results of that work agree with ours. As for the single-impurity case we reproduce the exponents of the power-laws (51) and (52) to leading order in U , i.e. the exponents of the extended LSGM are given by $1 - K$ and $2\alpha_B$, respectively. In the low-energy limit, the conductance exhibits the same scaling behavior as a function of T or δ_N , but for higher temperatures the T dependence of G at fixed N is much richer than the δ_N scaling, showing non-monotonic behavior and power-laws with different exponents in a variety of temperature regimes.

2. $T > 0$

Shortly after the discussion of resonant tunneling on asymptotically small scales the conductance for intermediate to high energies was investigated within a field-theoretical model using different approximate methods.¹⁷

For symmetric barriers and applying second-order perturbation theory in the barrier height the $T > 0$ deviations of $G_p(T)$ (at resonance) from e^2/h were determined to scale as T^{2K} .¹⁷ At further increasing T a regime of uncorrelated sequential tunneling (UST) was predicted based on a perturbative analysis in the inverse barrier height, where $G_p(T) \propto T^{\alpha_B - 1}$ and $\sigma(T) \propto T$.^{17,20} This regime is bounded from above by the (non-interacting) level spacing of the dot $\delta_{N_D} = \pi v_F / N_D$. Within the same perturbative approach and for $\delta_{N_D} \ll T \ll B$, $G_p(T)$ increases as $T^{2\alpha_B}$ for increasing T .¹⁷ In contradiction to the temperature dependence following from UST, in recent transport experiments on carbon nanotubes a suppression of G_p with decreasing T was observed for $T \lesssim \delta_{N_D}$.⁴⁸ Using another approximation scheme, “correlated sequential tunneling” (CST) was predicted to replace UST.^{21,27} It leads to $G_p \propto T^{2\alpha_B - 1}$. Although a simplified field-theoretical model of spinless fermions was used and contacts as well as leads were ignored the CST scaling was argued to be consistent with the experimental data. This consideration has stimulated a number of theoretical works.^{23–26} In particular, Quantum Monte Carlo (QMC) results²⁶ for $G_p(T)$ were interpreted to be consistent with CST for $T \lesssim \delta_{N_D}$. Resonant tunneling was also investigated using the “leading-log” method.^{24,25} Within this approach no indications of a CST regime were found.

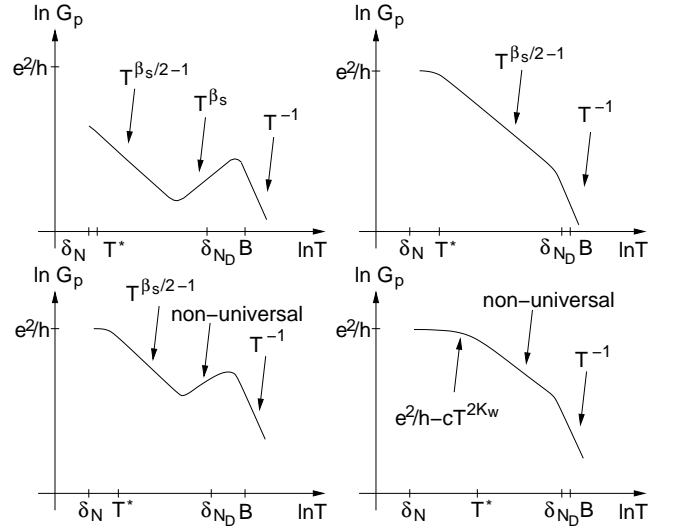


FIG. 14: Schematic plot of the different regimes for the scaling of the conductance G_p at resonance for symmetric barriers found using our approximation scheme. The upper left panel is for dots with a large number of lattice sites N_D and high barriers, the upper right for small N_D and high barriers, the lower left for large N_D and low barriers, and the lower right for small N_D and low barriers. The relevant energy scales are the band width B , the $U = 0$ level spacing of the dot δ_{N_D} , the lower bound of the UST regime T^* [see Eq. (53)], and the infrared cutoff δ_N associated with the number of lattice sites forming the interacting wire.

Being applicable for any barrier height, but only for interactions such that $1/2 \leq K \leq 1$, our fRG based

method is complementary to the approaches of Refs. 17 and 20. It has the advantage that all relevant temperature regimes can be investigated within one approximation scheme (see Ref. 40 and below).

In Fig. 14 our findings for $G_p(T)$ and a fixed N presented in Ref. 40 are summarized schematically in the four limiting cases of small and large quantum dots separated from the rest of the interacting wire by high and low barriers. The T^{-1} behavior found for scales of the order of B and larger is the same band effect as discussed above for the single-impurity case.

For large dots and high barriers (upper left panel of Fig. 14) the T^{-1} behavior is followed by a T^{β_s} scaling, with the strong-single-impurity exponent β_s , down to temperatures slightly less than δ_{N_D} . According to Eq. (32) in this parameter and temperature regime $G_p(T)$ is obtained by adding the resistances of the two individual barriers (Kirchhoff's law). Both follow the single impurity scaling T^{β_s} which explains that the same exponent is found in resonant tunneling. For even lower T , G_p follows a power-law with (to leading order in U) the UST exponent $\beta_s/2 - 1$ down to a scale T^* . The crossover from the regime in which Kirchhoff's law can be applied to the UST regime is relatively sharp and takes typically half an order of magnitude (see Fig. 2 of Ref. 40). For $T \ll \delta_{N_D}$ the width of $-df/d\varepsilon$ is smaller than δ_{N_D} and only a single resonance peak (the one around 0) of $|t(\varepsilon, T, \delta_N)|^2$ contributes to the integral in Eq. (16). The width $\Delta^{(\alpha)}$ of this peak vanishes as $\tau^2 T^{\beta_s/2}/N_D$ leading to $G_p(T) \propto T^{\beta_s/2-1}$ as discussed in Sect. III. In the case of hopping barriers τ stands for $t_{l/r}$ while it is proportional to $1/V_{l/r}$ for site barriers. The lower bound of this scaling regime is reached when T is equal to $\Delta^{(\alpha)}$, i.e. at

$$T^* \propto (\tau^2/N_D)^{1/(1-\beta_s/2)}. \quad (53)$$

Using Eq. (16) it is easy to see that for $T^* \ll T \ll \delta_{N_D}$ the half-width σ of the resonance in $G(T)$ as a function of V_g scales like T . These results hold for all cases in which we find a UST regime, i.e. for the other dot parameters discussed next, but also for asymmetric barriers and the off-resonance scaling investigated further below. For large dots, high barriers, and the values of N used here, T^* is very close to the scale δ_N . Below this scale no interaction-dependent ‘‘universal’’ behavior can be observed.

For small dots and high barriers (upper right panel of Fig. 14) δ_{N_D} and B are very close to each other and no regime with T^{β_s} scaling is developed. Due to the factor $1/N_D$ in Eq. (53), for small dots T^* is larger than for large N_D . For small dots a UST regime with exponent $\beta_s/2 - 1$ is not as nicely developed as for large N_D (see Fig. 2 of Ref. 40 and Figs. 16, 17, and 18 below).

For large dots but low barriers (lower left panel of Fig. 14) T^* moves to higher energies because of the factor τ in Eq. (53). Between B and δ_{N_D} , G_p decreases with decreasing temperature. As is discussed in Ref. 40 this decrease is not described by a power-law. We thus denote it as non-universal behavior.

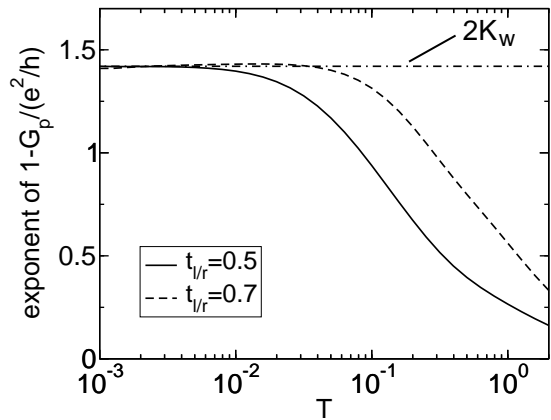


FIG. 15: Effective exponent (i.e. logarithmic derivative) of $1 - G_p(T)/(e^2/h)$ for a small dot with $N_D = 1$, $U = 1$, $N = 10^4$, and intermediate to weak hopping barriers $t_{l/r}$. Dashed-dotted line: $2K_w$.

For small N_D and low barriers (lower right panel of Fig. 14) δ_N and T^* are sufficiently separated so that we can observe an additional temperature regime with power-law scaling of G_p and an interaction-dependent exponent as exemplified in Fig. 15 for $U = 1$, $N = 10^4$, $N_D = 1$, and the barrier heights $t_{l/r} = 0.5$ as well as $t_{l/r} = 0.7$. We find that for $\delta_N \ll T \ll T^*$, $G_p(T)$ approaches e^2/h as

$$1 - G_p(T)/(e^2/h) \propto T^{2K_w}, \quad (54)$$

with the fRG approximation K_w for K obtained from β_w (see Sect. V A). In this temperature regime and for energies ε which contribute to the integral in Eq. (16), $|t(\varepsilon, T, \delta_N)|^2$ does not depend on T . We find that for $\delta_N \ll \varepsilon \ll T^*$, $\varepsilon - \varepsilon_\alpha - 2\Omega^{(\alpha)}(\varepsilon, 0, \delta_N) \propto \varepsilon$ and $\Delta^{(\alpha)}(\varepsilon, 0, \delta_N) \propto \varepsilon^{-\beta_w/2}$. Evaluating the ε integral for $\delta_N \ll T \ll T^*$ leads to Eq. (54). For low barriers, small N_D , and $T^* \ll T \ll \delta_{N_D}$ we no longer find the UST power-law but instead non-universal behavior.

For the cases in which a comparison is possible the above exponents agree (to leading order in U) with the results obtained for a field-theoretical model using perturbation theory in the barrier height and the inverse barrier height.^{17,20} In addition applying the fRG to our microscopic model we can describe the complete crossover between the temperature regimes with ‘‘universal’’ power-laws and cover the parameter regimes with non-universal behavior.

We do not find any indications of the CST exponent $2\alpha_B - 1$. Besides the single- and double-barrier problems some of us also studied transport of correlated electrons through junctions of M 1d wires, e.g. Y-junctions with $M = 3$ and X-junctions with $M = 4$.⁶⁰ Also in these geometries one finds power-law scaling of the conductance. For a certain case (Y-junction with magnetic flux) the K -dependent exponent is known analytically,⁶¹ which we again reproduce to leading order in U .⁶⁰ We thus conclude that in all cases of inhomogeneous TLLs we have

studied and in which exact results for exponents (from effective field-theoretical models) of power-law scaling are known we reproduce these exponents at least to leading order. We find it thus very likely that the occurrence of the CST regime with exponent $2\alpha_B - 1$ is an artifact of the approximations used in Refs. 21 and 27.

As Fig. 3 of Ref. 40 shows, the non-universal behavior discussed above might quite easily be identified incorrectly as power-law scaling with an exponent, which is significantly smaller than $\beta_s \approx 2\alpha_B$, i.e. in the vicinity of $2\alpha_B - 1$. This is of particular importance for the interpretation of noisy QMC data as well as noisy experimental results, both typically restricted to a temperature regime of one to two orders of magnitude.^{26,48} In Fig. 4 of Ref. 26 a single set of QMC data with $K = 0.6$, for an intermediate dot size, and intermediate barriers is presented roughly falling into the parameter regime shown in the lower left panel of Fig. 14. In Ref. 26 a certain part of the temperature regime with decreasing $G_p(T)$ (for decreasing T) was fitted by a power-law with exponent $2\alpha_B - 1$ which was then interpreted to support the occurrence of CST.

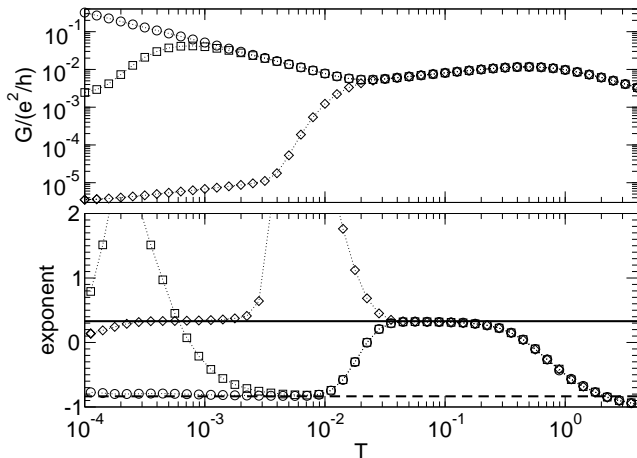


FIG. 16: Upper panel: $G(T)$ for symmetric barriers with $V_{l/r} = 10$ for $U = 0.5$, $N = 10^4$, $N_D = 100$ at resonance $|\Delta V_g| = 0$ (circle), very close to a resonance with $|\Delta V_g| = 0.001$ (squares), and in a conductance minimum with $|\Delta V_g| = 0.04$ (diamonds). Lower panel: Logarithmic derivative of $G(T)$. Solid line: β_s ; dashed line: $\beta_s/2 - 1$.

We next discuss the T dependence of the conductance away from V_g^r still considering symmetric barriers. In the upper panel of Fig. 16 $G(T)$ is shown for $U = 0.5$, $N = 10^4$, a large dot with $N_D = 100$, high barriers with $V_l = V_r = 10$, and three different $|\Delta V_g|$. Results for the resonance closest to $V_g = 0$ are shown. We have verified that similar behavior can be found for the other resonances. The circles show the conductance at $|\Delta V_g| = 0$. The peak conductance $G_p(T)$ displays the power-laws discussed above. This is best seen in the lower panel in which the logarithmic derivative of the conductance is shown. Close to the resonance (squares) for decreasing T , $G(T)$ follows $G_p(T)$ into the UST regime before the

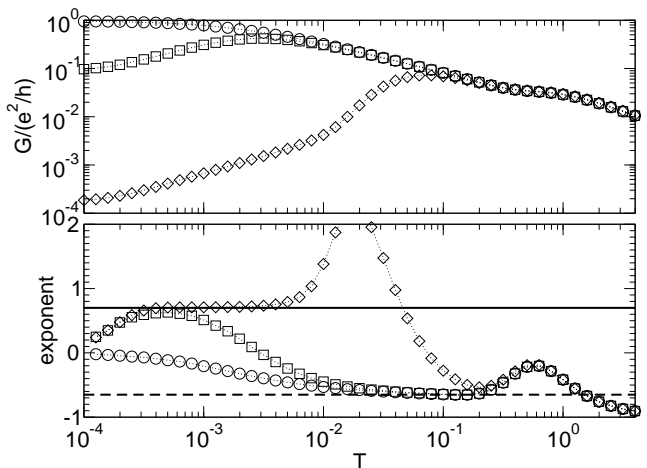


FIG. 17: Upper panel: $G(T)$ for symmetric barriers with $t_{l/r} = 0.2$ for $U = 1$, $N = 10^4$, $N_D = 4$ at resonance $|\Delta V_g| = 0$ (circle), close to a resonance with $|\Delta V_g| = 0.005$ (squares), and further away from the resonance with $|\Delta V_g| = 0.1$ (diamonds). Lower panel: Logarithmic derivative of $G(T)$. Solid line: β_s ; dashed line: $\beta_s/2 - 1$.

conductance at $|\Delta V_g| \neq 0$ decreases while $G_p(T)$ tends towards e^2/h . For $|\Delta V_g| \neq 0$ the peak in $|t(\varepsilon, T, \delta_N)|^2$ is centered around ΔV_g . In the UST regime its width still scales as $\Delta^{(\alpha)} \propto \tau^2 T^{\beta_s/2}/N_D$ (see Eq. (27) and above). As long as $|\Delta V_g| \ll \delta_{N_D}$ the curves separate when $\Delta^{(\alpha)}$ is equal to $|\Delta V_g|$. This leads to the “off-resonance” temperature scale

$$T_{\text{or}} \propto (N_D |\Delta V_g| / \tau^2)^{2/\beta_s}, \quad (55)$$

at which the off-resonance conductance separates from $G_p(T)$. Sufficiently away from the resonance, e.g. in the conductance minimum (diamonds), the temperature regime in which Kirchhoff’s law can be applied is followed by a regime in which the double barrier acts as a strong single impurity. This crossover typically takes one order of magnitude in T and consists of a drop of G by at least two orders of magnitude. In both these regimes $G(T)$ follows a power-law with exponent β_s , which arises for completely different reasons. The origin of the power-law for $\delta_{N_D} \leq T \ll B$ has been explained above. For these temperatures many peaks in $|t(\varepsilon, T, \delta_N)|^2$ contribute to the ε integral in Eq. (16). The single-impurity scaling on asymptotically small scales can be understood as follows: Off resonance and close to the chemical potential $|t(\varepsilon, T, \delta_N)|^2$ behaves like $(\varepsilon^2 + T^2)^{\beta_s/2}$ (for $\varepsilon, T \gg \delta_N$). In the evaluation of the integral in Eq. (16) the derivative of the Fermi function can be considered as being a constant (as a function of ε) which scales like $1/T$. The remaining integral with integrand $(\varepsilon^2 + T^2)^{\beta_s/2}$ runs over an energy range of order $2T$ which then leads to $G(T) \propto T^{\beta_s}$. For $T \lesssim \delta_N/2$ a deviation from the described power-law scaling sets in. As an additional example for the off-resonance behavior, in Fig. 17 we show

$G(T)$ for $U = 1$, $N_D = 4$, $N = 10^4$, weak hopping barriers with $t_{l/r} = 0.2$ (again the interaction across the barriers is set to 0) and three different $|\Delta V_g|$.

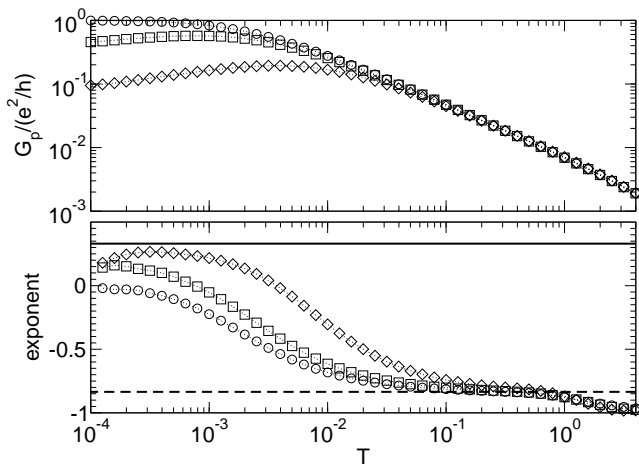


FIG. 18: Upper panel: $G_p(T)$ for asymmetric barriers with $U = 0.5$, $N = 10^4$, $N_D = 2$, and $V_l = 7$, $V_r = 12.3$ (squares) as well as $V_l = 4$, $V_r = 13.6$ (diamonds). For comparison also the symmetric case with $V_l = V_r = 10$ is shown (circles). Lower panel: Logarithmic derivative of $G_p(T)$. Solid line: β_s ; dashed line: $\beta_s/2 - 1$.

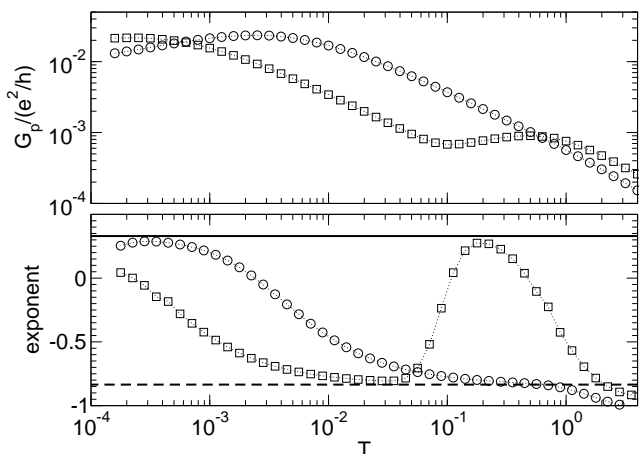


FIG. 19: Upper panel: $G_p(T)$ for asymmetric barriers with $V_l = 5$, $V_r = 50$, $U = 0.5$, $N = 10^4$, $N_D = 2$ (circles) and $N_D = 20$ (squares). Lower panel: Logarithmic derivative of $G_p(T)$. Solid line: β_s ; dashed line: $\beta_s/2 - 1$.

We finally describe the T -dependence of the conductance for asymmetric barriers at resonance. In Fig. 18 results are presented for $U = 0.5$, $N_D = 2$, $N = 10^4$, and different site barriers with weak to intermediate asymmetry $V_l = 7$, $V_r = 12.3$ (squares) and $V_l = 4$, $V_r = 13.6$ (diamonds). The combination of $V_{l/r}$ was chosen such that at high temperatures the curves approximately collapse. For comparison also the symmetric case with $V_l = V_r = 10$ is shown (circles). Over a wide range of temperatures $G_p(T)$ for asymmetric barriers shows the same behavior as in the symmetric case. The scale T_{as} on which $G_p(T)$ for $V_l \neq V_r$ starts to deviate from the behavior of the symmetric case discussed

above decreases with vanishing asymmetry parameter $\gamma = |V_l^2 - V_r^2|/(V_r^2 + V_l^2)$. In addition T_{as} decreases for increasing N_D as can be seen in Fig. 19 which shows $G_p(T)$ for $U = 0.5$, $V_l = 5$, $V_r = 50$, $N = 10^4$ and two different N_D . Even for a fairly strong asymmetry with $\gamma \approx 0.98$ ($V_l = 5$, $V_r = 50$) for $N = 10^4$ we observe the asymptotic low-energy behavior $G_p(T) \propto T^{\beta_s}$ only for very small N_D (see Fig. 19). Already for $N_D = 20$, $T_{as} < \delta_N$.

The temperature dependence of the conductance for asymmetric barriers and $V_g \neq V_g^r$ can be deduced from $G_p(T)$ obtained in the last paragraph (asymmetric barriers) and $G(T)$ for symmetric barriers at $|\Delta V_g| > 0$ discussed further above.

VI. SUMMARY AND PERSPECTIVES

In this paper we presented a method to calculate the linear conductance through inhomogeneous TLLs connected to semi-infinite non-interacting leads. The system is described by a microscopic lattice model of spinless fermions. As applications we studied transport in the presence of a single impurity as well as the double-barrier problem, allowing for resonant tunneling. The contacts are modeled to be smooth, i.e. in the absence of impurities and for $T \ll B$ the conductance is equal to e^2/h . This requires that the interaction is turned on smoothly close to the two contacts. The transport problem was previously investigated using effective field-theoretical models. In the cases where exact results for such models are known we obtained quantitative agreement for weak to intermediate interactions with $1/2 \leq K \leq 1$. At half-filling this corresponds to nearest-neighbor interactions $0 \leq U \leq 2$, which covers the whole parameter regime in which the model is a TLL (with $K < 1$). Away from half-filling even larger U can be considered.

Our method captures the expected power-law scaling of the conductance for a single weak and strong impurity. In addition, we can describe the complete crossover governed by a K -dependent one-parameter scaling function. For a single impurity we briefly studied attractive interactions. Also in this case our method provides reliable results for not-too-strong interactions with $1 \leq K \leq 3/2$, i.e. at half-filling for $-1 \leq U \leq 0$.

For resonant tunneling depending on the parameters of the quantum dot we find several temperature regimes with power-law scaling as well as non-universal behavior. All these temperature regimes are obtained within the same approximation scheme. The crossover between the regimes can be studied in detail. For parameters for which a comparison is possible our results agree with the ones obtained in lowest order perturbation theory in the barrier height and inverse barrier height. We do not find any indications of a ‘‘correlated sequential tunneling’’ regime with the exponent $2\alpha_B - 1$ predicted from an approximate Master-equation approach.^{21,27} If it would be present our method should be able to reveal such a

regime with a scaling exponent which is of leading order in the interaction.

Our method is a very flexible tool to investigate models of inhomogeneous TLLs. It allows for extensions which are required to obtain a more realistic description of experimental systems: (i) The spin degree of freedom can be included. (ii) Models with more realistic contacts (extended bulk and end contacts) can be treated. After projecting out the non-interacting leads the microscopic details of the contacts enter the fRG flow equations as the initial condition of the self-energy. Preliminary results show that imperfect leads have a strong effect on $G(T)$ even in cases in which the imperfection is fairly weak. (iii) More realistic models for the leads can be used. All that enters the fRG approach is the local Green function of the lead at the contact after disconnecting the lead and interacting wire. In addition the transport through junctions of interacting wires, such as Y - and X -junctions, as well as transport through Aharonov-Bohm geometries can be described using the fRG.

Acknowledgments

We thank M. Salmhofer and H. Schoeller for valuable discussions and U. Schollwöck for collaboration during the early stage of this research project. While completing this work all of us attended the *Winter School on Renormalization Group Methods for Interacting Electrons* at the *International Center of Condensed Matter Physics* of the University of Brasília, Brazil. We benefited from the possibility to discuss the issues presented here during the workshop. We thank A. Ferraz and the staff of the ICCMP for their hospitality. X.B.-T. was supported by a Lichtenberg-Scholarship of the “Göttingen Graduate School of Physics”.

Appendix

The Kubo formula for the conductance has a contribution with bare current operators and one with current-

vertex corrections. In this appendix we explain why the latter vanish in our approximation, consistent with the Ward identity.

We have approximated the full two-particle interaction vertex Γ by a renormalized nearest-neighbor interaction which is independent of frequency. Then the flow of the right current vertex $\Lambda_R(\omega + i0)$ is of order ω and vanishes in the limit of the dc conductance. The approximation that Γ is frequency independent has another consequence: by the flow equation, it follows that $\text{Im } \Sigma = 0$, that is we do not capture inelastic processes at second order in the interaction. They could be included in the flow equation by retaining the frequency dependence of Γ .

However, the fact that the vertex corrections and $\text{Im } \Sigma$ vanish simultaneously shows that our approximation is at least consistent with the Ward identity associated with particle number (charge) conservation. The global continuity equation for the interacting region is $\partial n_C / \partial t + J_R - J_L = 0$, where n_C is the total particle number in the interacting region, and $J_{L,R}$ are the currents entering the system from the left and leaving it to the right. This continuity equation implies a Ward identity.⁵⁷ After analytical continuation to frequencies slightly above and below the real axis (the branch cut of the current operators and the self-energy), the density response drops out and we obtain

$$P_R(\epsilon + i0, \epsilon - i0) - P_L(\epsilon + i0, \epsilon - i0) = 2 \text{Im } \Sigma(\epsilon + i0),$$

where $P_{L,R}$ are the corrections of the left and right current vertices, using the notation of Ref. 57. Thus, the current-vertex corrections are related to the discontinuity across the real axis of the self-energy. At $T = 0$, both sides vanish exactly because there is no inelastic scattering, while at finite temperatures, neglecting inelastic processes is a consistent approximation.

* Xavier B.-T. passed away in a tragic traffic accident on August 15, 2004.

¹ For a review on Tomonaga-Luttinger liquid behavior see K. Schönhammer, in *Interacting Electrons in Low Dimensions*, Editor: D. Baeriswyl, Kluwer Academic Publishers (2004); cond-mat/0305035.

² A. Luther and I. Peschel, Phys. Rev. B **9**, 2911 (1974).

³ D.C. Mattis, J. Math. Phys. **15**, 609 (1974).

⁴ W. Apel and T.M. Rice, Phys. Rev. B **26**, 7063 (1982).

⁵ T. Giamarchi and H.J. Schulz, Phys. Rev. B **37**, 325 (1988).

⁶ C.L. Kane and M.P.A. Fisher, Phys. Rev. Lett. **68**, 1220 (1992); Phys. Rev. B **46**, 7268 (1992); Phys. Rev. B **46**,

15233 (1992).

⁷ A. Furusaki and N. Nagaosa, Phys. Rev. B **47**, 4631 (1993).

⁸ K. Moon, H. Yi, C.L. Kane, S.M. Girvin, and M.P.A. Fisher, Phys. Rev. Lett. **71**, 4381 (1993).

⁹ D. Yue, L.I. Glazman, and K.A. Matveev, Phys. Rev. B **49**, 1966 (1994).

¹⁰ P. Fendley, A.W.W. Ludwig, and H. Saleur, Phys. Rev. Lett. **74**, 3005 (1995).

¹¹ I. Safi and H.J. Schulz, Phys. Rev. B **52**, R17040 (1995).

¹² D.L. Maslov and M. Stone, Phys. Rev. B **52**, R5539 (1995).

¹³ V.V. Ponomarenko, Phys. Rev. B **52**, R8666 (1995).

¹⁴ D.L. Maslov, Phys. Rev. B **52**, R14368 (1995).

¹⁵ A. Furusaki and N. Nagaosa, Phys. Rev. B **54**, R5239

- (1996).
- ¹⁶ R. Egger, H. Grabert, A. Koutouza, H. Saleur, and F. Siano, *Phys. Rev. Lett.* **84**, 3682 (2000).
 - ¹⁷ A. Furusaki and N. Nagaosa, *Phys. Rev. B* **47**, 3827 (1993).
 - ¹⁸ C. Chamon and X.G. Wen, *Phys. Rev. Lett.* **70**, 2605 (1993).
 - ¹⁹ I. Safi, *Phys. Rev. B* **56**, R12691 (1997).
 - ²⁰ A. Furusaki, *Phys. Rev. B* **57**, 7141 (1998).
 - ²¹ M. Thorwart, M. Grifoni, G. Cuniberti, H. Postma, and C. Dekker, *Phys. Rev. Lett.* **89**, 196402 (2002).
 - ²² T. Kleinmann, F. Cavaliere, M. Sassetti, and B. Kramer, *Phys. Rev. B* **66**, 165311 (2002).
 - ²³ A. Komnik and A.O. Gogolin, *Phys. Rev. Lett.* **90**, 246403 (2003); *Phys. Rev. B* **68**, 235323 (2003).
 - ²⁴ Y.V. Nazarov and L.I. Glazman, *Phys. Rev. Lett.* **91**, 126804 (2003).
 - ²⁵ D.G. Polyakov and I.V. Gornyi, *Phys. Rev. B* **68**, 035421 (2003).
 - ²⁶ S. Hügler and R. Egger, *Europhys. Lett.* **66**, 565 (2004).
 - ²⁷ M. Thorwart, R. Egger, and M. Grifoni, *cond-mat/0407751* (2004).
 - ²⁸ M. Salmhofer, *Renormalization*, (Springer, Berlin, 1998).
 - ²⁹ D. Zanchi and H. J. Schulz, *Phys. Rev. B* **61**, 13609 (2000); C. J. Halboth and W. Metzner, *ibid.* **61**, 7364 (2000); C. Honerkamp, M. Salmhofer, N. Furukawa, and T. M. Rice, *ibid.* **63**, 035109 (2001).
 - ³⁰ R. Hedden, V. Meden, Th. Pruschke, and K. Schönhammer, *J. Phys.: Condensed Matter* **16**, 5279 (2004); C. Honerkamp, D. Rohe, S. Andergassen, and T. Enss, *Phys. Rev. B* **70**, 235115 (2004).
 - ³¹ C. Wetterich, *Phys. Lett. B* **301**, 90 (1993).
 - ³² T. R. Morris, *Int. J. Mod. Phys. A* **9**, 2411 (1994).
 - ³³ M. Salmhofer and C. Honerkamp, *Prog. Theor. Phys.* **105**, 1 (2001).
 - ³⁴ V. Meden, W. Metzner, U. Schollwöck, and K. Schönhammer, *Phys. Rev. B* **65**, 045318 (2002).
 - ³⁵ V. Meden, W. Metzner, U. Schollwöck, and K. Schönhammer, *J. of Low Temp. Physics* **126**, 1147 (2002).
 - ³⁶ S. Andergassen, T. Enss, V. Meden, W. Metzner, U. Schollwöck, and K. Schönhammer, *Phys. Rev. B* **70**, 075102 (2004).
 - ³⁷ V. Meden and U. Schollwöck, *Phys. Rev. B* **67**, 035106 (2003).
 - ³⁸ V. Meden, S. Andergassen, W. Metzner, U. Schollwöck, and K. Schönhammer, *Europhys. Lett.* **64**, 769 (2003).
 - ³⁹ V. Meden and U. Schollwöck, *Phys. Rev. B* **67**, 193303 (2003).
 - ⁴⁰ V. Meden, T. Enss, S. Andergassen, W. Metzner, and K. Schönhammer, *Phys. Rev. B* **71**, 041302(R) (2005).
 - ⁴¹ S. Tarucha, T. Honda, and T. Saku, *Solid State Com.* **94**, 413 (1995)
 - ⁴² M. Bockrath, D. Cobden, J. Lu, A. Rinzler, R. Smalley, L. Balents, and P. McEuen, *Nature* **397**, 598 (1999).
 - ⁴³ Z. Yao, H. Postma, L. Balents, and C. Dekker, *Nature* **402**, 273 (1999).
 - ⁴⁴ O. Auslaender, A. Yacoby, R. de Picciotto, K. Baldwin, L. Pfeiffer, and K. West, *Phys. Rev. Lett.* **84**, 1764 (2000).
 - ⁴⁵ M.S. Fuhrer, J. Nygård, L. Shih, M. Forero, Y.-G. Yoon, M. Mazzone, H. Coi, J. Ihm, S. Louie, A. Zettl, and P. McEuen, *Science* **288**, 494 (2000).
 - ⁴⁶ C. Papadopoulos, A. Rakitin, J. Li, A. Vedenev, and J. Xu, *Phys. Rev. Lett.* **85**, 3476 (2000).
 - ⁴⁷ R. de Picciotto, H. Stormer, L. Pfeiffer, K. Baldwin, and K. West, *Nature* **411**, 51 (2001).
 - ⁴⁸ H. Postma, T. Teepen, Z. Yao, M. Grifoni, and C. Dekker, *Science* **293**, 76 (2001).
 - ⁴⁹ We consider spinless TLLs connected to semi-infinite Fermi-liquid leads, which implies that the impurity free conductance is given by e^2/h .
 - ⁵⁰ F.D.M. Haldane, *Phys. Rev. Lett.* **45**, 1358 (1980).
 - ⁵¹ J.R. Taylor, *Scattering Theory*, John Wiley and Sons, New York, 1972.
 - ⁵² This can easily be shown by calculating the necessary integral by the theorem of residues.
 - ⁵³ For a review on the Landauer-Büttiker approach to transport see: S. Datta, *Electronic Transport in Mesoscopic Systems*, Cambridge University Press, Cambridge, 1995.
 - ⁵⁴ Due to renormalization the effective hopping matrix elements $\tilde{t}_{l/r}$ considered in Sect. III are not necessarily the same as the bare hoppings $t_{l/r}$ of Sect. II.
 - ⁵⁵ Due to renormalization the effective gate voltage \tilde{V}_g considered in Sect. III is not necessarily the same as the bare gate voltage V_g of Sect. II.
 - ⁵⁶ It is a finite T generalization of the $T = 0$ algorithm presented in Ref. 36.
 - ⁵⁷ A. Oguri, *J. Phys. Soc. Japan* **70**, 2666 (2001).
 - ⁵⁸ We will present a detailed study of the role of more realistic contacts in an upcoming publication.
 - ⁵⁹ For $\tilde{V} \neq 0$, i.e. off resonance, the resulting single site dot can be understood as a single impurity.
 - ⁶⁰ X. Barnabé-Thériault, A. Sedeki, V. Meden, and K. Schönhammer, *cond-mat/0411612* (unpublished).
 - ⁶¹ C. Chamon, M. Oshikawa, and I. Affleck, *Phys. Rev. Lett.* **91**, 206403 (2003).